When rare earth meets carbon nanodots: mechanisms, applications and outlook

Mengzhen Zhang,[a,b] Xinyun Zhai,*[a] Mingzi Sun,[c] Tengfei Ma,[a] Yongkang Huang,[a] Bolong Huang,*[c] Yaping Du*[a] and Chunhua Yan[a,d,e]

Rare earth (RE) elements are widely used in luminescent and magnetic fields by virtue of their abundant 4f electron configurations. Whereas, the overall performance and aqueous stability of single component RE materials need to be urgently improved to satisfy the requirements for multifunctional applications. Carbon nanodots (CNDs) are excellent nanocarriers with abundant functional surface groups, excellent hydrophilicity, unique photoluminescence (PL) and tunable features. The RE-CNDs hybrids combine the merits from both RE and CNDs, which dramatically enhance the holistic properties such as luminescent and magnetic-optical imaging performances, leading to highly promising practical applications in the future. Nevertheless, a comprehensive review focusing on the introduction and in-depth understanding of RE-CNDs hybrid materials has not been reported yet. This review endeavors to summarize the recent advances of RE-CNDs, including the interaction mechanisms, general synthesis strategies and applications of RE-CNDs in fluorescence, biosensing and multimodal biomedical imaging. Finally, we put forward the current challenges and the possible application perspectives of the newly developed RE-CNDs materials. We hope this review will inspire new design ideas and valuable references in this promising field in the future.

1. Introduction

Rare earth (RE) is the collective name of the 17 metallic elements consisting of the lanthanide series (La-Lu) as well as scandium (Sc) and yttrium (Y) in the periodic table. The gradual occupation of 4f orbitals makes them promising materials with unique mechanical, chemical, optical and magnetic properties, showing widespread applications in industrial and technological areas.[1] Nowadays, with the burst of nanoscience and nanotechnology, RE-doped nanomaterials play an even more important role in modern science and are considered to be one of the most promising materials in nanophysics, nanochemistry, nanomedicine, etc. RE-doped nanomaterials have special physicochemical properties while remaining the intra-configurational transitions and line-type spectra regardless the change of size and shape, which are superior to their bulk counterparts.[2] Retrospecting the booming of RE elements after the discovery about two centuries ago, the RE nanomaterials have been vital components of high-tech products and advanced materials, which are precious strategic resources all over the world.[3] However, singular RE nanoparticles fail to fulfill the stringent requirements for the multi-functionality of advanced materials. Along with the irreplaceable role and limited crust reserves of RE, RE hybrid functional nanomaterials are becoming the research focus.[4]

For over a decade, rare earth-carbon nanodots (RE-CNDs) hybrid nanomaterials have attracted increasing attention due to their prominent properties and versatile applications in biological analysis, chemical science and biomedical areas (Fig. 1). Carbon nanodots (CNDs) are referred to the kind of surface-passivated nano-sized carbon materials (typically less than 10 nm) with discrete, quasi-spherical morphology, different from the graphene quantum dots (GQDs) which are anisotropic with larger lateral dimensions than the height.[5-8] Plenty of reviews have focused on the properties of carbon-based dots whose two typical advantages are their strong photoluminescence (PL) and abundant surface groups. The PL properties of CNDs are excitation-wavelength dependent, which can be modulated by particle size and surface states (doping and surface functionalization).[9, 10] The versatile and easily modified functional groups on CNDs make them excellent nanocarriers with great hydrophilicity and biocompatibility, and most importantly, modifiable and tunable features. Based on these, CNDs have been applied in biomedicine, [11-13] cancer therapy, [14] electroanalytical, [15] electrochemiluminescence, [16]energy storage and conversion, [8], etc. The RE-CNDs hybrids combine the merits from both RE and CNDs, showing attractive and comprehensive properties, especially the luminescence and magnetic-optical imaging performance. Till now, a variety of nanomaterials have been reported as the building units of RE hybrid nanomaterials, such as noble metal (Au and Ag) nanoparticles, [17] magnetic nanoparticles (Fe_3O_4), [18] semiconducting polymer dots, [19] luminescent semiconductor quantum dots (QDs), [20] carbonaceous nanomaterials (e.g. graphene, carbon nanotube, fullerene and CNDs), [21, 22] etc. Among them, CNDs, after being first prepared by Xu. *et. al.* in 2004, have garnered intensive public interest in the past dozen years for their superior properties over other materials. In the field of bioimaging and biosensing, the conventional metal nanoparticles and QDs often suffer from severe intrinsic flaws, such as the toxicity of cadmium and selenium, and sophisticated and costly preparation routes;[23, 24] besides these, polymer dots and organic molecules are limited by poor

[a] *Tianjin Key Lab for Rare Earth Materials and Applications, Center for Rare Earth and Inorganic Functional Materials, School of Materials Science and Engineering & National Institute for Advanced Materials, Nankai University, Tianjin, 300350, China.*
[b] *College of Chemistry, Nankai University, Tianjin, 300350, China.*
[c] *Department of Applied Biology and Chemical Technology, The Hong Kong Polytechnic University, Hong Hum, Kowloon, Hong Kong, China.*
[d] *Beijing National Laboratory for Molecular Sciences, State Key Laboratory of Rare Earth Materials Chemistry and Applications, PKU-HKU Joint Laboratory in Rare Earth Materials and Bioinorganic Chemistry, College of Chemistry and Molecular Engineering, Peking University, Beijing, 100871, China.*
[e] *College of Chemistry and Chemical Engineering, Lanzhou University, Lanzhou 730000, China.*

photostability and potential toxicity. In comparison, CNDs can be easily fabricated from graphite or organic molecules,[12, 25] and possess more desired advantages in terms of their tunable PL, robust chemical inertness, photostability, hydrophilicity and good biocompatibility.[26] Compared with other traditional carbon nanomaterials, CNDs are also intriguing alternatives for their ultrafine sizes, tunable functional groups on the surface and facile synthesis process. These superior physicochemical properties of CNDs provide versatile functions for RE-CNDs, such as multiple luminescence, surface modifiability and great biocompatibility, which have great potential in the near future.

Among all the application areas of RE, RE luminescent and magnetic materials are extraordinary candidates that have been appealing to increasing scientists in the past decades. By virtue of the unique 4f electron configurations, RE luminescent materials have characteristic line-type emission bands, excellent photostability, long luminescent lifetime and large Stokes/anti-Stokes shifts. Whereas, the 4f-4f transitions of RE ions often suffer from low absorption coefficient and narrow absorption band arising from the parity forbidden 4f transitions, which dramatically limit their luminescent intensity. The synthesis of RE complexes is an effective strategy to enhance the luminescent efficiency, while it still has inherent disadvantages of poor thermal-stability and photobleaching.[27] Instead, the inorganic material CNDs have superior photo-, thermal- and chemical stability, and more importantly, they have the resistance to photo-bleaching and -blinking,[26] which endow RE-CNDs hybrids with improved luminescent stability and better processibility than pure molecular RE complexes.

The vital advantage of RE-CNDs is the integration of the merits in the luminescence of both rare earth and CNDs, which not only improves the performances but also extends the modal of luminescence. The intensive attentions on the CND for luminescence applications arise from their prominent features such as facile preparation, high chemical stability and photostability, remarkable water solubility and biocompatibility. [28] However, the luminescence properties of CND are relatively limited to the blue-green emission and the strong self-absorption induced quenching are their main shortcomings.[29, 30] The RE ions have shown unique luminescence properties with sharp emission, long life-time, high quantum yield and flexible tunability. Therefore, with the combination of RE and CND, the strong and tunable emission is expected to realize, which can also further extend the modal of luminescence probes. Such a combination significantly enriches the potential functions of the RE-CNDs such as supplying more comprehensive and accurate diagnosis information beyond conventional magnetic resonance imaging (MRI)/fluorescent imaging (FI).[31] Therefore, the integration of RE and CNDs enables the “one plus one is greater than two” effect and actualize the boost of luminescence properties for broad applications.

As for the RE magnetic materials, Gd^{3+} has been considered to be the most effective T_1-weighted contrast agent for magnetic resonance imaging (MRI). One of the most serious limitations of Gd^{3+} as MRI contrast agents is their toxicity towards biological systems, which has been solved by introducing chelation agents to stabilize Gd^{3+}. However, Gd-based complexes still have the problem of the leakage of Gd^{3+}, which inhibits the calcium channels and induce nephrogenic system fibrosis in patients who have renal dysfunction.[32] One alternative approach to suppress Gd^{3+} release is to encapsulate Gd^{3+} into an inorganic nanoparticle carrier while maintaining the T_1 contrast quality.[33] Examples of nanocarriers include semiconductor QDs,[34, 35] silica,[36] CaF_2, [37] Fe_3O_4,[38] and Gd_2O_3 nanoparticles,[39, 40] etc. Compared with them, CNDs bear ultrafine sizes and better biocompatibility, which not only protect Gd^{3+} from the harsh environment and remain superior T_1 contrast ability but also reduce the leakage of Gd^{3+} effectively. Moreover, the ultra-small size of CNDs allows the excretion from the body efficiently. Therefore, all of the abovementioned merits make this brand-new RE-CNDs material one of the most competitive candidates for practical applications in MRI imaging in the future.

A lot of research concerning the design and fabrication of RE-CNDs were reported in the past decades, coming up with many creative and inspiring combination strategies. In general, the RE-CNDs are obtained by the three following ways: (1) Utilizing the direct interactions between RE ions and the functional groups on the surface of CNDs; (2) Connecting CNDs with RE ions through organic ligands “bridge”; (3) Encapsulating CNDs and RE ions into an inorganic or polymer matrix. Notably, the unique properties and potential applications of this hybrid material are strongly dependent on their compositions and preparation strategies, which underscores the significance of the in-depth, comprehensive understanding of the rational structure-to-function design, efficient synthesis routes and versatile applications.

Although the special properties of RE and the unique photophysical properties of the CNDs have been intensively studied, the research of RE-CNDs hybrids remains in the early stage and still requires subsequent explorations. In this present review, we will summarize the latest advances of RE-CNDs in the past ten years and give a systematic review of the interior mechanisms, design strategies and different application directions of RE-CNDs hybrid nanomaterials. Novel design ideas and combination modes will be demonstrated and the potential applications in the field of optics, bioanalysis, chemical sensing and magnetic-optical imaging will be discussed. More notably, the reported intrinsic interaction mechanisms of the hybrid nanomaterials are elucidated. This is the first review presenting an overview of this novel RE-CNDs. We firmly believe that this review will provide novel ideas from the

design to the multiple subsequent applications of RE-CNDs, which will inspire more scientists to the development of this brand-new material in both fundamental research and industrial applications, thus benefits the whole human society in the future.

2. Interaction Mechanisms for RE-CNDs Hybrids

2.1. Mechanism study in luminescent RE-CNDs

2.1.1. Optical properties of RE and CNDs. The unique optical properties of RE ions are primarily attributed to their 4f electron configurations. The large atomic numbers bestow them a large variety of electronic energy levels and dynamics of electronic transitions, with nearly 30,000 observable spectral lines for instance.[41] The most common oxidation state of RE elements is the trivalent RE ions, hereafter RE^{3+}, because of their greatest stability. The 4f orbitals are shielded by the filled $5s^25p^6$ subshells, which protect these 4f energy levels from the crystalline field and external chemical environment.[42, 43] As a result, the rich 4f-4f transitions, which cover the entire spectrum from ultraviolet (UV), visible light to near-infrared (NIR) emissions, display narrow and recognizable emission bands, large Stokes shifts and long lifetime of the excitation states. From the aspect of intrinsic transition pathways, the luminescent mechanisms of RE^{3+} are typically classified into three types: PL, quantum cutting, and upconversion (UC). The activators of PL, including mainly Eu^{3+}, Tb^{3+}, Sm^{3+} and Dy^{3+}, have abundant emission spectra spanning the whole visible region under UV excitation. For quantum cutting, high-energy excitation is also required and then transfer to two or more low-energy photons with emissions. UC instead, is triggered by photons with lower energy (in most cases NIR light) to create upconverting high-energy emissions.

With the trend of nanoscience and interdisciplinarity, RE luminescent materials in nanoscale have emerged. The unique physical and chemical properties of RE-doped nanomaterials, such as highly controllable size and morphology, as well as easy modification by biomolecules, impart them with excellent performance in diagnosis, imaging and treatment.[4, 44] Therefore, RE-doped nanomaterials are able to serve as multifunctional platforms and have been regarded as the most promising materials in biomedical applications.

The unique optical properties of CNDs are mainly discussed from three aspects: absorbance, PL and photo-stability. CNDs have strong optical absorption in the UV region and a shoulder peak extends to the visible region (Fig. 2). Typically, the absorption band at around 250-300 nm belongs to the π-π^* transitions of aromatic C-C bonds in CNDs, while the shoulder band is known as the n-π^* transitions of C=O bonds or other surface groups.[5, 6] The excellent PL is one of the most fascinating properties of CNDs, in which the mechanism has been under debate since its discovery. CNDs have unique excitation wavelength-dependent PL behaviour and broad emission profile. The tunable PL property endows CNDs with more selectable emissions through tuning the excitation wavelength. Although the exact PL mechanism remains unsettled, it is comprehensively accepted that the PL emissions of CNDs are mainly originated from two classes, one is the intrinsic state emissions caused by the bandgap transitions in carbon core, and the other is the defect state emissions associated with the surface defects of CNDs.[8, 45] The fluorescence from the carbon core states derives from the isolated conjugated π-domains, while that from the surface states are mainly correlated with unperfect surface defects.[45] Only the surface-derived emissions located in the visible region are bright enough for efficient emissions, which can be attributed to the recombination of electron-hole pairs on the surface.[46] Thus, the surface states have a more efficient impact on the optical performance of CNDs than the core states. Therefore, it is crucial to utilize the surface passivation and modification to modulate the PL of CNDs and increase the quantum yield. The interactions between RE^{3+} and the surface groups of CNDs cause great effects on the PL properties of CNDs, for example, the decrease or quenching of the fluorescence. The fluorescent change endows RE-CNDs with adjustable fluorescent properties, which significantly paves their applications in chemical and biological sensing.

2.1.2. Mechanisms of Energy Transfer in RE-CNDs. The luminescent RE-CNDs are mainly utilized from two aspects: one is based on the energy transfer between RE^{3+} and CNDs, the other is taking advantage of the dual-mode luminescence from both RE^{3+} and CNDs.

Ever since discovered by Weissmann in 1942, people realize that the excitation to RE^{3+} in the presence of organic ligands results in the metal-centred luminescence ("antenna effect").[47] The sensitization of RE^{3+} is attributed to the complex energy transfer process which contains several energy transition pathways.[42] This phenomenon leads us to explore the possible energy transfer processes existing in RE-CNDs when RE^{3+} combines with the surface groups of CNDs. Generally, the CNDs have strong absorption in the UV region and mainly exhibit the emission colours of blue or green.[8] Previous research has proven that CNDs act as both superior electron donors and electron acceptors under photo-excitation.[48] The RE^{3+} are hard Lewis acid and good acceptors for the energy transfer, which is the prerequisite of the energy transfer from CNDs to RE^{3+}. On the other hand, the high surface positive charge density of RE^{3+} as hard Lewis acid results in more tendency to combine with hard binding sites containing large electrostatic components like the anionic ligands carboxylates, phosphinates, phosphonates and β-diketonates.[49] Therefore, the abundant

functional groups (carboxylates, hydroxyl, etc.) on the surface of CNDs provide plenty of binding sites to facilitate the formation of RE-CNDs hybrids.

Among other RE^{3+}, Eu^{3+} and Tb^{3+} are the most studied activators with intensive emissions located in the visible region because they are less affected by the high-energy vibrations and have the largest quantum yields.[50] The red emissions of Eu^{3+} are located in ~615 nm by the $^5D_0 \rightarrow {}^7F_2$ transitions and the green emissions of Tb^{3+} are mainly located in ~550 nm by the $^5D_4 \rightarrow {}^7F_5$ transitions. Most of the experimental and theoretical research of the energy transfer process within RE-CNDs in recent years are based on Eu-CNDs or Tb-CNDs. Therefore, the proposed energy transfer phenomenon and mechanisms in Eu- and Tb-CNDs are summarized and evaluated below.

It has been widely accepted that there are direct energy transfers from CNDs to Eu^{3+}/Tb^{3+}, which were preliminarily postulated from the observation of CNDs luminescent quenching upon introducing Eu^{3+}.[51-54] In 2011, Zhao *et al.* reported the quenching effect and decreased lifetime of CNDs upon the addition of Eu^{3+}. They attributed this phenomenon to the disruption of the radiative recombination on CNDs surface induced by Eu^{3+}, with possible charge- or energy transfer process.[51] After that, Dong and co-workers proposed a possible Förster resonance energy transfer (FRET) mechanism from CNDs to Eu^{3+}/Tb^{3+} (Fig. 3A).[55] The occurrence of the FRET process has two requirements, one is the integral spectral overlap between the emission of donor fluorophore and the excitation of acceptor molecule, the other is the close distance (1-10 nm) between donor and acceptor.[56, 57] The speculation in this work was proposed based on the close distance achieved by the coordination between RE^{3+} and polyol functional groups on CNDs surface. These fluorescence quenching phenomena are closely related to the variation of surface states on CNDs.

Therefore, to further demonstrate the energy transfer mechanism, the optical properties of CNDs must be taken into consideration. As mentioned in the last section, the surface states have a more significant impact on the optical performance of CNDs. Hence, the disruption of the CNDs surface states by Eu^{3+} may play an important role in the quenching effect of CNDs. Pallavi Singhal *et al*. observed a higher quenching effect on surface states than the carbon core states of CNDs caused by Eu^{3+} and contributed it to the influence of both electron transfer and aggregation to the surface states of CNDs.[54] They conducted a steady-state PL experiment and found a faster decay of the intensity in carbon surface states than in core states upon the addition of Eu^{3+}. The subsequent time-resolved emission studies suggested a faster decay trace in both core states and surface states of CNDs with the addition of Eu^{3+} compared with that of pure CNDs, which verified the electron transfer from CNDs to Eu^{3+}. Similarly, the results also showed a larger decay trace in surface states, which was in accordance with the steady-state luminescence study. Considering the distance-dependent property of the electron transfer process, it is speculated that the electron transfer process existed in Eu-CNDs was caused by the direct interactions between Eu^{3+} and surface groups of CNDs (Fig. 3B and 3C(a)), which lead to the quenching effect on both core states and surface states of CNDs. Whereas, the aggregation of CNDs caused by Eu^{3+} was also responsible for the quenching of the surface states (Fig. 3C(b)), which was confirmed by the direct binding of Eu^{3+} with carboxyl groups on the surface of CNDs through XPS analysis. Therefore, both the electron transfer and aggregation of CNDs contributed to the quenching of the surface states, leading to a faster luminescence quenching than that of the core states.

2.1.3. Mechanisms of Energy Transfer in RE-CNDs with matrix. From another point of view, CNDs are superior sensitizers for the luminescent RE^{3+}. In the aforementioned situations, the energy transfer within RE-CNDs can induce the fluorescence quenching of CNDs but without the emissions of RE^{3+}. This is due to the fact that the excitation state of RE^{3+} couples with the high-energy vibration of O-H in the aqueous solution, leading to the quenching of RE^{3+} luminescence.[58] Hence, this underscores the significance of specific design strategies to minimize non-radiative deactivation. From this aspect, the most useful way is to create a rigid environment around RE^{3+},[50] such as incorporating them into a host matrix.[59] Taken the CNDs/YF_3: RE^{3+} (RE = Eu or Tb) for example, the energy transfer mechanism is described in Fig. 4A. Under the excitation of UV light, the electrons of CNDs transfer from π to π* energy level. Then the electrons on the LUMO level of C relaxed to the N π* level (the N elements on CNDs are derived from the precursor urea) and the O π* level. Part of these electrons transferred to the π level of C with blue emissions, while the other transferred to Eu^{3+}, leading to the characteristic luminescence of Eu^{3+} (i.e. the transitions of $^5D_0 \rightarrow {}^7F_J$, J = 0, 1, 2). Meanwhile, the energy on the $^5D_{1\text{-}4}$ levels of Eu^{3+} is recaptured by CNDs, named electron capture (EC), and then delivered to the $^5D_0$ level of Eu^{3+} through a FRET process. As a result, the electrons on the $^5D_0$ level of Eu^{3+} are greatly accumulated and caused the enhancement of emission intensity.[60]

The evidence of the energy transfer process is also shown in CNDs/LaF_3:Eu^{3+}, where greatly enhanced emissions of Eu^{3+} were achieved with the addition of CNDs during the synthesis process of LaF_3:Eu^{3+}.[60] The doped CNDs acted as the sensitizer through the energy transfer from CNDs to Eu^{3+}, which was verified by the broadband of CNDs in the excitation spectrum (right inset of Fig. 4B) and the fairly weak emissions of the pure LaF_3:Eu^{3+} (Fig. 4B). The authors proposed that the energy transfer has been ascribed to the FRET and provided evidence for support. One is the spectral overlap exhibiting between the emission bands of CNDs and the excitation bands of LaF_3:Eu^{3+} (right inset of Fig. 4B). The other is the increased lifetime of Eu^{3+} monitored at 612 nm when doping with CNDs (λ_{ex} = 340 nm).[61]

It is noteworthy that the fabrication methods and the combination modes in the matrix are essential for the successful energy transfer because simply physical mixing CNDs and LaF_3:Eu^{3+} cannot obtain intensive Eu^{3+} emission. The same results were observed in CNDs/$ZnGa_2O_4$:Eu^{3+}, where adding CNDs during the fabrication process of $ZnGa_2O_4$:Eu^{3+} enhanced the emission intensity of Eu^{3+} while the physical mixture of CNDs and $ZnGa_2O_4$:Eu^{3+} displayed no emission from Eu^{3+}.[62]

Another energy transfer process of WO_4^{2-}→Ln^{3+}⇆CNDs was reported by Huang and co-workers. They observed a luminescent enhancement in flower-like $MgWO_4$:Eu^{3+} by the introduction of CNDs. The luminescent intensity of CNDs-incorporated $MgWO_4$:Eu^{3+} increased by 4 times compared with bare $MgWO_4$:Eu^{3+}. They attributed this to the energy transfer process exhibiting between CNDs and Eu^{3+}.[63] Then in another work, they further investigated the PL mechanism of the synthesized CNDs@$MgWO_4$:Ln^{3+} (Ln^{3+} = Eu^{3+} or Tb^{3+}). As shown in Fig. 4C and D, upon the introduction of CNDs, dramatically enhanced PL intensity was observed under the excitation of 263 nm. The emission intensity of Eu^{3+} (λ_{em} = 614 nm) in CNDs@$MgWO_4$:12%Eu^{3+} enhanced by 2.5 times compared with pure $MgWO_4$:12%Eu^{3+}, and similar enhancement of Tb^{3+} was found in CNDs@$MgWO_4$:8%Tb^{3+} by 7 times compared with $MgWO_4$:8%Tb^{3+}. These fluorescence enhancements caused by the energy transfer process within the CNDs@$MgWO_4$:Ln^{3+} are shown in Fig. 4E. In brief, after the absorption of 263 nm UV light (the maximum excitation wavelength of WO_4^{2-}), the energy at the excited $^1B(^1T_2)$ level in WO_4^{2-} may undergo a resonance process to the $^5D_3$ level of Tb^{3+}. The energy at the $^5D_3$ level of Tb^{3+} undergoes two different pathways: a portion of the energy transfer to the excited states of CNDs and then go back to the $^5D_4$ level of Tb^{3+}, while the other was captured by the $^5D_4$ level of surrounded Tb^{3+} *via* the cross-relaxation. As a result, the energy at the $^5D_4$ level is extremely strengthened, leading to more efficient emissions from $^5D_4$ to ^7F_J (J = 3,4,5,6) energy levels of Tb^{3+}.[64]

Except for the direct energy transfer from CNDs to Eu^{3+}/Tb^{3+}, this process is also achieved with the participation of an intermediate ligand. The mechanism has been studied in case of the interaction between the europium–tetracycline (EuTC) complex and CNDs.[53] The EuTC complex does not have any luminescence upon the excitation of the optimal excitation and emission wavelengths of CNDs (i.e. λ_{ex} = 347 nm; λ_{em} = 421 nm). After adding EuTC complex into the CNDs solutions, the intensity of the characteristic Eu^{3+} emission at 614 nm (λ_{ex} = 347 nm) enhanced gradually, while the luminescence of CNDs was quenched at the same time. The quenching mode of CNDs by EuTC complex showed a deviation from the typical linear Stern-Volmer quenching, and conformed a quadratic relationship with the concentration of the quencher, which indicated the energy transfer between CNDs and EuTC.[65] To explore the inner energy transfer mechanism, the bandgap calculation for the PL of CNDs was conducted, which confirmed two types of emission bands of CNDs located at the wavelengths 419 nm and 436 nm, respectively. These are derived from the two different binding sites on the surface of CNDs: the citric acid-rich and glutathione-rich surface states originating from the carbonaceous precursors citric acid and glutathione, respectively. Therefore, the interactions between CNDs and EuTC lead to the splitting of conduction band (3.1 eV) in CNDs into two shallow levels (2.96 eV for 419 nm; 2.84 eV for 436 nm) (Fig. 4F). Upon excitation, the excited electrons in the conduction band of CNDs first entered into the shallow states, and then transferred to the singlet state of tetracycline (TC). The energy on the triple state of TC finally transferred to the triple state of Eu^{3+} and generated characteristic emissions.

Despite these previous research, the in-depth energy transfer mechanisms between RE^{3+} and CNDs remain to be further explored. From one aspect, the innate PL mechanism of CNDs are still under debate. On the other hand, evidence of the energy transfer process is mainly concentrated on the variation of luminescence spectra and decay curves. The lack of accurate calculations and characterizations of the energy levels and electron transition pathways within RE-CNDs limits their further improvements, which need further explorations and discussions in the future.

2.2. Mechanism study in magnetic-optical RE-CNDs

One of the core issues faced by biology and medicine is the demand for high-quality, high-contrast and real-time bioimaging techniques, which are crucial for a better understanding of the structure and properties in biological systems. Recently, bimodal and multimodal contrast agents, especially MRI/optical based contrast agents, have garnered increasing attention. The MRI imaging technique provides physiological distinctions at the tissue and organ level while the optical imaging technique reports pathologic information at the cellular or sub-cellular level.[66] Although each imaging technique has its own advantages, a single technique cannot meet all requirements. MRI has deep tissue penetration and high resolution, but its sensitivity at high magnetic field strength reduces greatly.[67] On the other hand, optical imaging has high sensitivity and resolution, while often suffers from the low transparency to tissues, especially at shorter wavelengths in the visible region (400-700 nm).[68] Therefore, the combination of these complementary imaging techniques will lead to greatly enhanced imaging accuracy and broader applications.

Nowadays, the utilization of advanced nanoparticles has been emerged as cutting-edge technology for multimodal imaging, achieving complementary and integrated imaging quality in clinical diagnosis.[69] The hybrid nanostructured Gd-CNDs afford the

paramagnetism of Gd^{3+} alongside with the fluorescence of CNDs, realizing excellent magnetic/optical multimodal imaging with enhanced general performances, which have untapped potential in biomedical areas. Moreover, the CNDs act as inert carriers to build up a platform integrating different imaging modalities with great stability in one biological system. In this section, the inner mechanisms and advantages of Gd-CNDs using in dual- or multi-modal imaging are systematically summarized as follows.

2.2.1. Introduction of MRI and contrast agents. MRI is one of the most effective imaging techniques in the biomedical area through providing important diagnostic and prognostic information with high anatomic contrast, spatial and temporal resolution as well as deep tissue penetration, which has been extensively explored in the past 30 years.[70] In addition, compared with X-ray computed tomography (CT) imaging, positron emission tomography (PET) and single-photon emission computed tomography (SPECT), the MRI technique is non-invasive, which does not apply radioactive agents or high-energy electromagnetic wave.[4, 68]

Considering the precise mechanisms of MRI have already been thoroughly studied and explained, herein we will introduce the essential rules of MRI for a better understanding of Gd-CNDs as the contrast agents. The MRI signals are produced *via* the resonance and relaxation processes of atom nuclei (in most cases hydrogen protons) in biological systems under the magnetic field. Upon exposure to the external magnetic field, the hydrogen protons nuclear spins are aligned either parallel or antiparallel with the direction of the magnetic field, inducing a net longitudinal magnetization. After adding a specific radio frequency (RF) pulse, the proton nuclear spins will be excited to generate transverse magnetization. Then, after the removal of RF pulse, the excited nuclei will return to the ground state through two independent relaxation processes: (i) the recovery of T_1 longitudinal relaxation and (ii) the decay of T_2 transverse relaxation. Based on these two processes, the MRI signals are categorized into two different imaging modes named T_1-weighted images and T_2-weighted images. The faster T_1 relaxation rate ($R_1 = 1/T_1$, s^{-1}) results in a brighter T_1-weighted image, and in contrast, a faster T_2 relaxation rate ($R_2 = 1/T_2$, s^{-1}) yields a darker T_2-weighted image.

Due to the limited sensitivity of MRI, the contrast agents are essential ingredients to increase the signal-to-noise (N/S) contrast between diseased and normal tissues. The enhancement of MRI signals is ascribed to the interactions between contrast agents and neighbouring water molecules, which shorten the T_1 or T_2 relaxation time of the water molecules. The performances of contrast agents are quantitatively evaluated by the longitudinal relaxivity (r_1) and the transverse relaxivity (r_2), which are referred to the normalization of R_1 or R_2 to the concentrations of metal ions, respectively.

2.2.2. Gd-CNDs as MRI contrast agents. Currently, a variety of MRI contrast agents have been investigated, including nanoparticles and metal complexes with central metal ions including Mn^{2+}, Fe^{2+}/ Fe^{3+}, Eu^{3+}, Gd^{3+}, etc.[71-73] Among others, the Gd-based contrast agents have been proven to be the most clinically available ones for T_1-weighted imaging.[66] Stemming from their high paramagnetism and long electron spin relaxation time, Gd^{3+} shortens the longitudinal relaxation time for improved T_1-weighted images and becomes excellent candidates for MRI in clinical applications.[74] However, free Gd^{3+} is highly toxic, which involves the metabolism of the human body.[75, 76] Therefore, the primary target is to prevent the leakage of Gd^{3+} from Gd-based contrast agents. The traditional Gd-based complexes are regarded as an effective strategy to address this problem. However, despite their improved properties and commercial availability, Gd-based complexes have been reported to cause severe nephrogenic systemic fibrosis (NSF) especially for patients with kidney dysfunction. What's more, Gd-based complexes have short *in vivo* circulation lifetimes and often suffer from high cost and low contrast efficiency.[77, 78] Recently, increasing attention has been focused on the fabrication of inorganic nanoparticles-based contrast agents. The nanoparticles are promising platforms with superior magnetic, optical and electronic properties, facile intracellular uptake and excellent *in vivo* stability.[79] Inspiring from the unique optical properties and biocompatibility, CNDs are promising nano-capsules/-carriers for the Gd-based contrast agents. With the combination of Gd^{3+} and CNDs, CNDs not only function as fluorescent probes, but also impart Gd-CNDs with much lower toxicity and great hydrophilicity, where the latter plays a significant role in enhancing the distribution of imaging agents in tissues and organs, and thus better penetration depth and spatial visualization are realized. Moreover, the ultrafine sizes and hydrophilicity of Gd-CNDs MRI contrast agents endow them with excellent renal clearance, which is of great importance to lower the safety risks for clinical applications.

For the rational design of Gd-CNDs as MRI contrast agents, the influence factors of the longitudinal relaxivity must be taken into consideration. The commonly used theory for the analysis of the relaxation process derives from the Solomon-Bloembergen-Morgan (SBM) equations.[66, 80-82] The longitudinal relaxivity are contributed by three types of interactions with water molecules: 1) the direct coordination with metal ions (inner-sphere), 2) the binding with ligands through hydrogen bond (second-sphere) and 3) the translational diffusions near ligands (outer-sphere). The observed relaxivity is given by Eq. (1).

$$r_1^{total} = r_1^{IS} + r_1^{SS} + r_1^{OS} \quad (1)$$

The equation has been proven to be qualitatively applicable to nanoparticles. The inner-sphere contribution is correlated with the core of nanoparticles dominates the inner-sphere interactions, while the second- and outer-sphere contributions are greatly influenced by the water-dispersible layer.[83-85] However, only the Gd^{3+} on the outer surface of nanoparticles are able to interact with water molecules and enhance the longitudinal relaxivity.[83] Therefore, efforts should be devoted to increasing the surface-

chelated Gd^{3+} in order to improve the general performance of Gd-CNDs in MRI. For example, Gd-DTPA-CNDs (DTPA–diethylenetriamine pentaacetic acid) were reported with the longitudinal relaxivity up to 56.72 mM^{-1} s^{-1}. The Gd^{3+} are directly chelated onto the outer surface of CNDs-DTPA, leading to the significant enhancement of the longitudinal relaxivity.[86] What's more, the ultrafine sized Gd-CNDs exhibit the enhanced surface-to-volume ratio, which increases the interactions between surface Gd^{3+} and water molecules.[87]

3. General synthesis strategies for RE-CNDs hybrids

Different fabrication methodologies have been developed to synthesize RE-CNDs with multiple functionalities, which significantly affect the properties and applications of RE-CNDs to a large extent. Therefore, in this section, a general introduction of synthesis strategies and various combination modes of luminescent and magnetic RE-CNDs are summarized and illustrated, respectively.

3.1. Synthesis methods of luminescent RE-CNDs

Generally, the luminescent RE-CNDs are fabricated either by simple one-step methods, or by multi-step methods including the direct coordination and the assistance with ligands. Different synthesis methods are shown in Table 1 and Table 2 and are demonstrated in the following. Besides, the RE-CNDs incorporated into the inorganic/polymeric matrixes are summarized subsequently.

3.1.1. One-step synthesis of luminescent RE-CNDs. As shown in Table 1, the luminescent RE-CNDs can be simply synthesized by one-step procedures, such as one-pot hydrothermal, heating, carbonization and microwave-assisted methods. These methods have the merits of simultaneously preserving the luminescence of both materials by adding RE^{3+} salts into the precursors of CNDs.[88-98] This kind of approach dramatically facilitates the characteristic emissions of RE^{3+} and realizes the multicolour luminescent properties. For example, Dong *et al.* introduced $EuCl_3 \cdot 6H_2O$ or $TbCl_3 \cdot 6H_2O$ into the polyethylene glycol 400 (PEG400) and conducted a heating process, the obtained Eu/Tb-CNDs emitted strong red and green luminescence, respectively.[55] Similarly, the RE-CNDs synthesized by incorporating $YbCl_3$ and $NdCl_3$ into citric acid and ethylenediamine showed unique NIR emissions.[90] Such a luminescence enhancement of RE^{3+} is closely related to the coordination environment around RE^{3+}. Those RE^{3+} added before the fabrication of CNDs bear more saturated coordination interactions while the simple mixing treatment will lead to unsaturated coordination centres, which are easily affected by the aqueous systems. Therefore, the one-step synthesis routes provide a simple and cost-effective way to obtain multi-luminescence from both CNDs and RE^{3+}, while they still have limitations when it comes to complicated structure, including the coordination and the combination with other inorganic or polymeric materials.

3.1.2. Multi-step synthesis of luminescent RE-CNDs. Besides the one-step fabrication, the luminescent RE-CNDs can be synthesized by versatile design ideas through the direct interactions between RE^{3+} and CNDs, with the assistance of ligands or by incorporating RE^{3+} and CNDs into a host matrix.

3.1.2.1 Combination by the direct coordination between CNDs and RE^{3+}. The simplest method is the direct mixing of the RE^{3+} and CNDs to achieve the incorporation of RE^{3+}. The synthesis routes of CNDs are well-known to be classified into two categories: "top-down" and "bottom-up".[7, 8, 45] In the fabrication of RE-CNDs, most of the CNDs are synthesized based on the "bottom-up" procedures, which supply much more abundant combination sites and functional surface groups through facile and mild synthesis conditions when compared with "top-down" methods.[8] Moreover, the CNDs obtained by "bottom-up" routes generally have higher quantum yield than that from "top-down" routes. The precursors in the "bottom-up" procedures are mainly small molecules or polymers, like citric acid, urea, L-lysine, etc, which undergo a simple procedure to form CNDs, such as hydrothermal, pyrolysis and microwave-assisted methods. Depending on different sources of precursors, CNDs contain various surface groups, including hydroxyl, carboxylic acid, amino, carbonyl, thiol and so forth.[9, 99] Therefore, plenty of binding sites induced by the abundant functional groups on CNDs demonstrate flexible and accessible combination with RE^{3+}, as well as other organic, polymeric, or biological ligands.

Owing to the facile surface modification, the surface groups (*e.g.*, carboxyl, hydroxyl, and amine groups) on CNDs directly interact with Eu^{3+} and Tb^{3+} to form RE-CNDs hybrids.[51, 54, 100-107] Through the simple synthesis routes, RE-CNDs display excellent hydrophilicity, biocompatibility and photostability in biological systems, which have great advantages for biological and chemical detection, such as the detection of phosphate,[51] fluoride ions,[54] dipicolinic acid (DPA),[100, 104, 106] ATP (adenosine disodium triphosphate),[108] guanosine 3'-diphosphate-5'-diphosphate (ppGpp),[105], etc.

3.1.2.2. Combination with the assistance of organic ligands. Some RE-CNDs were fabricated using a ligand as the bridge between CNDs and RE^{3+}. The ligands are connected to CNDs either by covalent interactions or by simple mixing of CNDs with RE complexes. Given the example for the covalent binding strategy, the diethylenetriamine pentaacetic acid dianhydride (DTPAda) reacts with the amino groups on the surface of CNDs and yield CNDs-DTPA, which further coordinated with Eu^{3+} to form CNDs-DTPA-Eu as a fluorescent probe.[109] Similarly, the CNDs-EDTA-Eu was prepared by a two-step surface functionalization of CNDs where EDTA covalently bound onto CNDs and subsequently coordinated with Eu^{3+}.[110] The sulfonyl chloride group of BHHCT–Eu^{3+} (BHHCT–4,4'-

bis(1'',1'',1'',2'',2'',3'',3''-heptafluoro-4'',6''-hexanedion-6''-yl)-chlorosulfo-o-terphenyl) also reacts with the amino groups on CNDs so that the Eu complexes are easily coupled onto CNDs (Fig. 5A).[89]

Besides, for the noncovalent combination, a ratiometric fluorescent probe CNDs-calcein-Eu^{3+} was synthesized by simply mixing CNDs, calcein and Eu^{3+}.[111] Another example of the non-covalent combination mode is by adding CNDs into RE complexes. The luminescent reinforcement of Ln^{3+} emission was reported in the Ln complex $Ln(tta)_3(H_2O)_2$ after the subsequent coordination with CNDs.[112] The 1-(2-thenoyl)-3,3,3- trifluoroacetone (tta) ligand acted as the sensitizer and coordinated with Ln^{3+} to form $Ln(tta)_3(H_2O)_2$ complex first, then the carboxyl groups on CNDs further coordinated with Ln^{3+} through the replacement of the two water molecules on $Ln(tta)_3(H_2O)_2$ complex (Fig. 5B).

Actually, the direct mixing of RE^{3+} with pre-synthetic CNDs often leads to the quenching of CNDs because of the energy transfer from CNDs to RE^{3+}, where the luminescence of RE^{3+} cannot be observed due to the vibration induced quenching in aqueous solution. Thus, the RE-CNDs fabricated by the direct coordination or with the ligand-assisted methods are mainly used in bioanalysis and ion detection.

3.1.2.3. Incorporating RE-CNDs into the inorganic matrix. Incorporating into an inorganic matrix is an effective way to create a rigid environment for RE^{3+} and enhance the stability of RE-CNDs hybrids. Various of combination methods have been conducted to fabricate RE/CNDs co-doped inorganic matrix.

Firstly, the RE-CNDs can be synthesized *in situ* upon the formation of the inorganic matrix. One of the synthesis strategies is the one-step *in situ* hydrothermal method, where all the precursors of CNDs, RE^{3+} and inorganic materials are mixed and undergo the same preparation process. Examples are the porous CNDs/hydroxyapatite:Eu,Gd (N-CNDs/HAp:Eu,Gd),[113] $Ca_{19}Mg_2(PO_4)_{14}:Ln^{3+}$ (Ln = Eu and/or Tb),[91] and CNDs/Eu^{3+}-LaF_3.[61] Another methodology is based on the combination of RE-CNDs after the CNDs synthesis. The CNDs are prepared in advance by the hydrothermal, microwave, pyrolysis methods, etc., and then incorporated into the precursors of the RE-doped host matrix or along with RE^{3+} into a common matrix during the preparation process. Typical examples are based on the metal-organic frameworks (MOFs). The CNDs are encapsulated into the Eu-centred MOFs with the emission from both CNDs and RE^{3+}, which has been used in the detection of Cu^{2+}, Cr^{6+} and water content.[114-116] Besides, RE^{3+} and CNDs can be co-doped into a common MOFs, such as CNDs/Eu@MOFs [117] and Tb^{3+}@p-CNDs/MOF [118]. Other inorganic matrixes have also been reported with the successful incorporation of CNDs during the preparation process, such as $YF_3:RE^{3+}$ (RE = Eu or Tb),[60] $MgWO_4:RE^{3+}$ (RE = Eu or Tb),[63, 64] and $ZnGa_2O_4:Eu^{3+}$.[62] It has also been reported that CNDs and $YVO_4:Eu^{3+}$ are incorporated into silica networks along with the detection target 4-NP (4-nitrophenol) *via* a simple sol-gel reaction. After removing the 4-NP template from silica matrix, a molecularly imprinted ratiometric fluorescent sensor was obtained with enhanced affinity to the template molecules and detection sensitivity.[119]

The second synthesis mode is introducing CNDs after the formation of RE^{3+} doped inorganic matrix. Zhuang's groups conducted a sol-gel method to embed CNDs into the silica layer outside the $NaYF_4$:Yb,Tm nanoparticles and realized the dual-mode luminescence of both UC and downconversion (DC) (Fig. 5C).[120] Similarly, $SrAl_2O_4$:Eu,Dy@CNDs,[121] $NaYF_4$:Eu@CNDs,[122] and $NaYF_4$:Yb,Er(Tm)@CNDs [59] were prepared using the same sol-gel method. Besides, through a simple stirring process, He and co-workers successfully embedded CNDs into the mesoporous $Al_2O_3:Eu^{3+}$ by means of the hydrogen-bond interactions.[123] Moreover, CNDs can be directly synthesized in the presence of the RE-doped inorganic matrix through the hydrothermal (CNDs/$NaLuF_4$:Yb,Er),[124] or solvothermal method ($NaYF_4$:Er,Yb(Tm)@CNDs).[125]

3.1.2.4. Incorporating RE-CNDs into the polymer matrix. Polymers are another type of attractive host material owing to their excellent features including the high processibility, mechanical strength, flexibility as well as the low cost. Introducing the two components RE complexes and CNDs with distinct optical characteristics into the polymer matrix is an effective way for the design and fabrication of luminescent polymer composite film with photo-adjustable properties. The RE-CNDs based polymers were mainly synthesized by the direct solution mixing or solution cast methods. Chen and co-workers embedded the $Eu(DBM)_3$, $Tb(DBM)_3$ (DBM: dibenzoylmethide) and CNDs into the poly(methyl methacrylate) (PMMA) to form a white-light-emitting polymer film *via* a simple solution mixing process.[126] The RE complexes dispersed well in PMMA owing to the interactions between RE^{3+} and the oxygen atoms on PMMA chains. The functional modification with methacrylate on CNDs also played an important role in the great compatibility of CNDs with PMMA. Another work based on $Eu(DPA)_3$ and $Tb(DPA)_3$ was conducted by mixing the RE complexes and CNDs into the poly(vinyl alcohol) (PVA) film with UV light-switchable properties.[127] The solution of the composite was also used as the specific inks for anti-counterfeiting applications. Except for the RE complexes, $EuCl_3$ and CNDs are also reported to be embedded into PVA film by the solution cast procedure.[128] The Eu^{3+}/CNDs/PVA film showed tunable PL, which has been used as the light conversion film to promote plant growth. This kind of novel polymer composite film with unique luminescence properties can be further extended and has great potential in optical devices, anti-counterfeiting and agricultural applications.[124] These RE-CNDs based hybrid materials have superior stability and great potential in luminescence and biosensing fields. However, most of the inorganic/polymer matrixes in those hybrids act as inert supporters lacking the interactions with RE-CNDs, which are to be resolved in the future.

3.2. Synthesis of magnetic-optical RE-CNDs

The RE-CNDs with magnetic-optical properties are mainly realized by the introduction of Gd^{3+}, as well as other RE^{3+} like Yb^{3+} and Ho^{3+}. Table 3 summarizes different fabrication methods of RE-CNDs with MRI/fluorescence imaging properties, which are described in detail as follows.

3.2.1. One-step synthesis of magnetic-optical RE-CNDs. Most of the reported magnetic-optical RE-CNDs are fabricated by the one-step method. Different from the fabrication procedures of luminescent RE-CNDs, where RE^{3+} can coordinate with CNDs directly, the formation of Gd-CNDs *via* direct interactions between Gd^{3+} and CNDs is difficult.[129] One of the main preparation procedures for Gd-CNDs is extremely simple *via* encapsulating the Gd source into the precursors of CNDs. The Gd sources include inorganic salts of RE (e.g. $GdCl_3$, $Gd(NO_3)_3{\cdot}6H_2O$, $HoCl_3$),[129-134] or RE complexes.[135, 136] Meanwhile, the synthesis procedures have been conducted using the one-step hydrothermal, pyrolysis, microwave-assisted hydrothermal and microwave-assisted polyol method (see Table 3). For example, Xu *et al.* prepared Gd-CNDs hybrid through a one-pot hydrothermal method from a mixture of citric acid, ethanediamine and $GdCl_3$. They proposed a three-stage formation process of Gd-CNDs, namely nucleation, growth and aggregation (Fig. 6A). In the precursor solution, the formation of Gd^{3+} complex prevents the precipitation. And the reaction was controlled in the growth stage in order to achieve the optimal performance of the hybrid material, where the embedded Gd^{3+} are stabilized through coordinating with the surface functional groups of neighbouring CNDs.[129] The Gd-CNDs synthesized by Bourlinos and co-workers were based on the gadopentetic acid (a chelate complex of Gd^{3+}) as the Gd source and tris(hydroxymethyl)aminomethane (Tris base) as the carbon source.[135] The two carboxylic groups on gadopentetic acid interact with Tris base to promote the homogeneous dispersion of Gd^{3+} in CNDs.

Similar synthesis strategies were also shown in the MRI/CT/fluorescence multi-mode Gd/Yb-CNDs imaging probes, where the inorganic salts or complex of Gd and Yb were introduced into the precursors of CNDs and then undergo a simple process to form Gd/Yb-CNDs (Fig. 6B).[87, 137]

Except for incorporating Gd^{3+} into the precursors of CNDs, Gd-CNDs can also be fabricated directly from Gd complexes. Chen and co-workers used a typical Gd complex Gd-DTPA as the precursor of both Gd^{3+} and CNDs to prepare Gd-CNDs *via* a calcination process, which had improved MRI efficiency and fluorescent property.[138] Similarly, Du's group also synthesized Gd-CNDs using Gd-DTPA as the precursor of Gd^{3+} and CNDs, and glycine as the passivation agent *via* a one-step hydrothermal method.[139] Ren *et al.* reported a one-step pyrolysis treatment to prepare Gd-CNDs, with the Gd complex – Gadopentetate monomeglumine (GdPM) as the precursor.[133]

However, one of the current obstacles for preparing Gd-CNDs is the difficulty of accurate size control. To overcome this, a novel mesoporous silica nanoparticle (MSN) -templated method was designed to obtain desired particle sizes, where MSN acted as the reactors for the one-step synthesis of Gd-CNDs.[140, 141] Through adding the precursors of Gd^{3+} and CNDs into MSN with different pore sizes and then undergoing a calcination process, Chen and co-workers obtained Gd-CNDs with the size of 3.0, 7.4 and 9.6 nm.[140] This synthesis method provides an example for the easy design and control of different sized Gd-CNDs with improved MRI/fluorescence imaging properties.

Generally, the one-step synthesis is the most effective and commonly used strategy to fabricate Gd-based CNDs, which can preserve great MRI and fluorescence abilities from Gd^{3+} and CNDs. The functional groups on the surface of CNDs provide abundant combination sites for further modification.

3.2.2. Multi-step synthesis of Gd-based CNDs. By virtue of the mediate ligands, Gd-CNDs are fabricated through the coordination between Gd^{3+} and the ligands linked to the surface of CNDs.[86] Shi and co-workers prepared a dual-mode imaging probe of Gd-DTPA-CNDs based on the coordination between Gd^{3+} and DTPA. They first fabricated amine-terminated CNDs by using branched polyethylenimine (PEI) as the source of amino groups for further modification. Then the cyclic DTPAda was covalently bound onto the surface of CNDs to form CNDs-DTPA. Finally, Gd^{3+} was introduced by simply adding $GdCl_3$ into the system, which interacts with DTPA directly. The synthesis routes are shown in Fig. 6C.

Through further combination with other materials, the Gd-CNDs enable extended properties. It has been reported that Gd-CNDs were covalently bound with the amino-functionalized Fe_2O_3.[132] The Gd-CNDs@Fe_2O_3 showed excellent PL property as well as the T_1 and T_2 MRI ability. However, the reports on multi-step synthesis methods for Gd-based CNDs are quite rare, partly because of the complicated procedures, and partly because of the high request of biocompatibility and low cytotoxicity for *in vivo* bioimaging. Hence, the precursors and fabrication processes are to be optimized for practical applications.

It is concluded that the different synthesis methods of Gd-based RE-CNDs provide valuable references for more flexible modification, inspiring scientists to explore advanced fabrication procedures to further improve the general performance of Gd-CNDs and achieve extended applications in biomedical imaging and other fields.

4. Applications of luminescent RE-CNDs

The unique optical properties of both RE^{3+} and CNDs in RE-CNDs hybrid nanomaterials enable the versatile luminescent performances such as the improved emission intensity, dual-mode luminescence and controllable emission colours. The luminescent RE-CNDs hybrids have two main applications: luminescent phosphors and fluorescent sensing probes. Thus, this section will comprehensively introduce these two applications.

4.1. Luminescent phosphors

Fundamentally, all the applications of luminescent RE-CNDs are determined by their unique optical properties. The energy transfer between CNDs and RE^{3+} enhances the characteristic luminescence of RE^{3+}, and the CNDs render the hybrids superior hydrophilicity and biocompatibility. Meanwhile, the RE-CNDs show the characteristic emissions from RE^{3+}, such as the red emission of Eu^{3+}, the green emission of Tb^{3+} and the white emission from the Eu^{3+}/Tb^{3+} co-coped CNDs. The remarkable and flexible luminescent properties of RE-CNDs allow them to be the most competitive candidates in the applications of multicolour luminescent phosphors.

As previously discussed, the energy transfer between RE^{3+} and CNDs render the RE-CNDs excellent synergistic interactions. The CNDs can act as the sensitizer of RE^{3+} to strengthen their characteristic emissions.[61] The most commonly used visible-emitting RE^{3+} are Eu^{3+} (red) and Tb^{3+} (green) since they are more resistant to the external disturbance of vibration and present higher luminescence purity.[50] Thus, the visible-emitting Eu^{3+} and Tb^{3+} are the most studied RE^{3+} in the combination with CNDs. Huang and colleagues observed a significant luminescence enhancement in the $MgWO_4:Eu^{3+}$ after doping with CNDs.[63] Similar enhancement was also detected in another work of the group.[64] Through the introduction of CNDs, the luminescence intensities of $MgWO_4:Eu^{3+}$ and $MgWO_4:Tb^{3+}$ are enhanced by 2- and 7-fold, respectively, which was attributed to the energy transfer between CNDs and $MgWO_4:RE^{3+}$ (RE = Eu or Tb). Furthermore, instead of the direct excitation of CNDs by UV light, CNDs also act as a sub-energy level to reinforce the UC characteristic emissions of RE^{3+}. This phenomenon was first reported by Xu *et al*. by introducing CNDs into the UC nanoparticles $NaYF_4$:Yb,Er(Tm).[59] Upon excitation, the CNDs mediate the energy transfer between different RE^{3+} to modulate the UC process, and as a result, the red and NIR UC emissions (λ_{ex} = 980 nm) were both reinforced. These intriguing results provided a novel strategy for the development of controllable UC materials with largely improved luminescence for the NIR imaging in the biomedical field.

From another point of view, the doped RE^{3+} also broadens the PL spectra of CNDs. As to the next generation of bioimaging, long-wavelength emissions are highly desired for their full-colour emission, less tissue damage and better tissue penetrability. With the research advances of CNDs in the past decades, the majority of PL from CNDs located in blue and green regions, whereas the CNDs with red-emissions are barely reported.[142, 143] In view of this, the introduction of RE^{3+} is a promising way to realize the multi-colour emissions in RE-CNDs. As an example, during the preparation of CNDs, the $TbCl_3{\cdot}6H_2O$ or $EuCl_3{\cdot}6H_2O$ were added into the polyol, such as PEG400, and then undergo a simple one-step heating process. The resulted Tb/Eu-CNDs have line-type green/red emissions with the quantum yields up to 85% and 75%, respectively (Fig. 7A).[55] The intense characteristic f-f transitions are ascribed to the FRET from CNDs to Tb^{3+}/ Eu^{3+}, which has been elucidated in the second section. The superior green/red luminescence of the RE-CNDs highlights the positive influence of synergistic interaction between RE^{3+} and CNDs.

However, despite the highly efficient energy transfer existed in Tb/Eu-CNDs, the fluorescence of RE^{3+} is easily quenched by the water due to the high-energy vibration of O-H bonds.[58] Based on this, an improved method was developed to synthesis the Eu-CNDs by a microwave heating (MW) process to weaken the quenching effect.[103] Compared with Eu-CNDs fabricated by the conventional heating methods with a strong quenching effect, the Eu-CNDs originated from the MW method bear more carboxylate groups on the surface of CNDs. This provides more binding sites for the coordination of Eu^{3+} and blocks the vibronic state of water, which shows intensive red luminescence of Eu^{3+} with the quantum yield of 18%.

One of the most important highlights of RE-CNDs is the combination of different luminescent centres, which dramatically broaden the possibilities of fabricating versatile and controllable luminescent phosphors. Owing to the high colour purity and stability, Eu^{3+} (red) and Tb^{3+} (green) are the most commonly used visible light emitting RE^{3+}. Together with the blue-emitting CNDs, the co-doping of Eu^{3+} and Tb^{3+} endow the RE-CNDs with three primary colours (i.e. RGB), which has great potential in the full-spectrum modulation including the white light emission. For example, the white light emitting Eu/Tb-CNDs is obtained *via* a simple hydrothermal process by adding $Eu(NO_3)_3{\cdot}6H_2O$ and $Tb(NO_3)_3{\cdot}6H_2O$ into the precursors of CNDs.[88] Nevertheless, an urgent challenge for the fabrication of multicolour luminescent phosphors is the quenching of RE^{3+} by O-H vibration in aqueous solution. The best approach to minimize the quenching effect is to create a rigid environment for RE^{3+},[50] like incorporating RE^{3+} and CNDs into an inorganic matrix. Xu *et al.* fabricated $NaYF_4$:Eu@CNDs nanocomposites by embedding CNDs in the silica layer on the surface of $NaYF_4$:Eu nanoparticles. The $NaYF_4$:Eu@CNDs had dual emissions from CNDs (blue) and Eu^{3+} (red), and the luminescence was adjustable by tuning the $NaYF_4$:Eu to CNDs ratios.[122] Liu and co-workers added the oxides of Eu and Tb into the precursors and

synthesized $Ca_{19}Mg_2(PO_4)_{14}:RE^{3+}$ (RE = Eu or Tb), in which the CNDs formed during the sol-gel preparation process. The nanocrystalline phosphors had the emissions of CNDs, Eu^{3+} and Tb^{3+}. By changing the types, concentrations and ratios of co-doped RE^{3+}, the phosphors had a broad range of emission colours from blue, green, pink, red to white. Similar luminescent phosphors with tunable emission colours were reported including RE-CNDs (RE = Eu^{3+} or Tb^{3+}), [102] CNDs/$ZnGa_2O_4:Eu^{3+}$,[62] and CNDs/$YF_3:RE^{3+}$ (RE = Eu or Tb).[60]

Except for the most commonly used Eu^{3+} and Tb^{3+}, there are also other RE^{3+} (e.g. Nd^{3+}, Sm^{3+}, Dy^{3+}, Er^{3+}, Tm^{3+} and Yb^{3+}) reported to combine with CNDs, rendering RE-CNDs more emission colours extending to the NIR region. Wu *et al.* added the Yb and Nd salts to the precursors of CNDs to form Yb^{3+} or Nd^{3+}-doped CNDs (Yb^{3+}/Nd^{3+}-CNDs).[90] The Yb^{3+}/Nd^{3+}-CNDs had the NIR emissions located in 998 nm and 1068 nm under the single UV excitation, respectively. In this hybrid, the CNDs acted as both the luminescence centre and the "antenna" for the PL of Yb^{3+} and Nd^{3+}. Shi's group successfully synthesized RE complex-functionalized CNDs, named RE-CNDs (RE = Eu^{3+}, Sm^{3+}, Er^{3+}, Yb^{3+}, Nd^{3+}), with the emission spectrum ranging from visible to NIR regions (λ_{em} = 400-1400 nm) under the excitation of visible light.[112]

When talking about RE, the conventional upconversion rare earth (UCRE) nanoparticles are crucial candidates that cannot be ignored. The RE-CNDs with the combination of UCRE nanoparticles and DC CNDs have the unique property of dual-mode luminescence. This was shown in the study by Xu *et al.*, where the fabricated $NaYF_4$:Yb,Tm@CNDs nanocomposites displayed green light-emission under 365 nm excitation and blue purple light-emission under 980 nm excitation.[120] This result provided a new idea for the combination of UC and DC luminescence in a single hybrid, which dramatically broadens the applications of UCRE in the biological field. The similar dual-mode PL was also observed in $NaLuF_4$:Yb,Er/CNDs reported by Zhou *et al*.[124] It is noteworthy that the $NaLuF_4$:Yb,Er/CNDs hybrids have also been used in the anti-counterfeiting and solid-state luminescence, suppressing the aggregation of CNDs in solid-state. The latter application has been ascribed to the effective adsorption and dispersion of CNDs on the surface of $NaLuF_4$:Yb,Er nanoparticles. Likewise, the doping of CNDs into the hydroxyapatite:Eu,Gd with porous structure (i.e. CNDs/HAp:Eu,Gd) also inhibited the aggregation of CNDs with effective dual emissions under the single excitation in solid states.[113]

To achieve better luminescent performance with mechanical robustness and processibility, the RE-CNDs are embedded into a polymer film. For instance, CNDs, RE complexes $Eu(DBM)_3$ and $Tb(DBM)_3$ (DBM–dibenzoylmethide) were incorporated into a PMMA film.[126] Through tuning the ratios between CNDs, $Eu(DBM)_3$ and $Tb(DBM)_3$, the composite polymer film possessed pure white emission (Fig. 7B and C, CIE coordinate at (0.31, 0.32)) under 400 nm excitation with the quantum yield up to 16.6%, while the polymer film was transparent under visible light (Fig. 7D). Fig. 7E showed the emission spectrum of the PMMA film with different luminescent centres. They also proposed the energy transfer mechanism of the white-emitting film, which is illustrated in Fig. 7F. In addition, the introduction of RE complex and CNDs enhances the thermal stability of PMMA film. Similar composite polymer films like CNDs/$Eu(DPA)_3$/$Tb(DPA)_3$-PVA (DPA–pyridine-2,6-dicarboxylic acid; PVA–poly(vinyl alcohol))[127] and CNDs/Eu^{3+}/PVA [128] are reported with multiple and tunable luminescence. Such composite polymer films can be applied in anti-counterfeiting, promotion of plant growth, etc., showing great potential in industrial and agricultural fields.

4.2. Fluorescent probes

One of the most intriguing applications of luminescent RE-CNDs is in the field of sensing owing to the PL properties of RE^{3+} and CNDs. The RE-CNDs fluorescent probes are designed based on the quenching/enhancement of fluorescence (off/on) or the ratiometric fluorescent sensing. It is noted that RE-CNDs as promising ratiometric fluorescent probes have attracted great attention over the past few years. Contrary to the probes based on a single luminescence, the ratiometric fluorophores have the unique self-calibrated property with at least two emission wavelengths under a single excitation, which effectively eliminates the interference from the environment and improve the detection sensitivity and precision. Therefore, we will discuss in the field of ratiometric fluorescent sensing as follows.

4.2.1. Biosensing. The RE-CNDs have been used in the detection of a variety of biomolecules with plenty of novel design ideas, mainly based on the interactions between analytes and RE^{3+} or CNDs.

Utilizing the analyte as the ligand with the "antenna" effect for the sensitization of RE^{3+} is an effective way for biosensing, where the CNDs act as the reference at the same time. A typical example is the detection of an anthrax biomarker–dipicolinic acid (DPA). Different carriers for RE^{3+} have been used in DPA detection, such as metal-organic frameworks (MOFs),[144] carbon nanotubes,[145] and solid films,[146] whereas their applications are often suppressed by the disruption from the environment and low stability under moisture conditions. In comparison, CNDs provide superior photostability and biocompatibility in biological systems, which is beneficial for the ratiometric fluorescent detection in aqueous solution.[94, 98, 100, 104, 106, 147, 148] Chen *et al.* designed a ratiometric fluorescent probe Tb-CNDs for DPA detection, with CNDs as the reference part and Tb^{3+} as the recognition and detection part (Fig. 8A).[100] The precursors ethylenediaminetetraacetic acid (EDTA) and triethylenetetramine (TETA) endowed CNDs with abundant carboxylate and amide surface groups to coordinate with Tb^{3+}. Before the titration of DPA, the PL spectra of Tb-CNDs under 275

nm excitation was dominated by the emission of CNDs and displayed blue luminescence (inset photographs in Fig. 8B). By increasing the concentration of DPA from 0.005 to 1.2 μM, the green emission peaks of Tb^{3+} enhanced gradually, owing to the efficient energy transfer from DPA to Tb^{3+}, while the luminescence of CNDs as the reference stayed constant (Fig. 8B). The probe had a low detection limitation of 5×10^{-9} M (much lower than 6×10^{-5} M – the infectious dosage of the *B. anthracis* spore), and the colorimetric change is even observed at the DPA concentration of 50 μM. Moreover, the Tb-CNDs was proved to have great selectivity without the interference from other aromatic acids and amino acids (Fig. 8C). A similar detection strategy for DPA was also developed in Eu-CNDs and CNDs/Eu^{3+}/GMP (GMP–5′-guanosine monophosphate disodium) system, where the red luminescence of Eu^{3+} has been greatly enhanced after the binding with DPA while the blue emission of CNDs remained steadily.[94, 98, 104, 147]

In another report, Qin *et al.* employed CNDs/ Eu^{3+}@MOFs to the recognition and detection of diaminotoluene (TDA), which is also based on the CNDs as the reference and Eu^{3+} as the detection fluorophore.[149] TDA is a metabolite reliable biomarker of toluene diisocyanates (TDI) which is an important industrial aliphatic compound. After CNDs and Eu^{3+} are encapsulated into the MOFs, the carboxylate groups on the surface of CNDs coordinate with Eu^{3+} and act as the "antenna" to sensitize the luminescence of Eu^{3+} (λ_{ex} = 308 nm). Then the presence of TDA weakly coordinated with Eu^{3+} and cause the decrease of emissions from Eu^{3+} *via* the N-H vibrations of TDA. The CNDs/Eu^{3+}@MOFs probe had high water tolerance and acid-base sensitivity, which have great potential for the practical detection of TDA in human urine.

Instead of the sensitization of RE^{3+}, Li and co-workers constructed a molecularly imprinted (MIP) sensor CNDs/YVO_4:Eu@MIP for the detection of non-fluorescent 4-nitrophenol (4-NP) with CNDs as the analyte sensitive fluorophore and YVO_4:Eu as the reference.[119] The probe had dual luminescence with the blue-emissive CNDs (470 nm) and red-emissive Eu^{3+} (617 nm) under the excitation of 330 nm, where the luminescence of CNDs was selectively quenched by 4-NP. This probe has been successfully used in tap water and human urine samples, which is promising for environmental monitoring and water quality evaluations in the future.

The abovementioned examples are used for the detection of a single biomolecule species, except for that, the rational design of the RE-CNDs fluorescent probes realize the sensitive response to two different targets with a single probe. Zhou *et al.* developed a novel fluorescent probe CNDs-DTPA-Eu by using analyte as the sensitizer for the red luminescence of Eu^{3+}, which realize the fluorescence "switch-off" and "switch-on" upon the addition of TC and H_2O_2 in turn.[109] The DTPA was covalently bound onto CNDs and then coordinated with Eu^{3+} to form CNDs-DTPA-Eu. The additional TC coordinated with Eu^{3+} to form CNDs-DTPA-EuTC and acted as the sensitizer of Eu^{3+}, quenching the blue emission from CNDs due to the static quenching effect. Meanwhile, no emissions from Eu^{3+} has been noted because of the vibrations from neighbouring water molecules. Subsequently, the added H_2O_2 bound with CNDs-DTPA-EuTC *via* replacing the coordinated water molecules of the complex, leading to greatly enhanced red luminescence of Eu^{3+} (Fig. 8D). The PL spectra of the CNDs-DTPA-Eu with the addition of TC and subsequent H_2O_2 are shown in Fig. 8E and F, respectively. More importantly, the CNDs-DTPA-Eu fluorescent probe has merits of non-toxicity, low detection limits and great biocompatibility, which satisfies the requirements of effective intracellular detection (Fig. 8G). The above results verified the potential of RE-CNDs nanoprobes in the practical diagnosis. However, differentiability and sensitivity are challenges that need to be further improved in the future.

4.2.2. Chemical sensing. Ion detection is of great significance because some ions are highly toxic and have a potential influence on the human body as well as the environment. One of the earliest examples of RE-CNDs for ion sensing is the detection of phosphate (Pi).[51] Zhao and colleagues designed an "off-on" ratiometric fluorescent probe based on Eu-CNDs for the successful detection of Pi in a complex artificial wetland system (Fig. 9A). Firstly, upon the addition of Eu^{3+} into the CNDs solution, Eu^{3+} coordinated with the abundant carboxylate groups on the surface of CNDs and acted as a bridge to cause the aggregation of neighbouring CNDs. As a result, the fluorescence of CNDs at 420 nm is gradually quenched with more Eu^{3+} (turn-off) through the energy transfer between Eu^{3+} and CNDs. The Stern-Volmer constant (K_{SV}) of the quenching of CNDs by Eu^{3+} was calculated to be ~1.3×10^5 M^{-1}, indicating the high quenching efficiency. Secondly, the presence of Pi disassociated the aggregated CNDs again, leading to the recovery of the fluorescence (turn-on). The luminescence recovered to 93% of the initial intensity of untreated CNDs. The off-on fluorescence switching is able to observe by naked eyes (inset photographs in Fig. 9B and C) when adding Eu^{3+} and Pi subsequently (Fig. 9B and C). The detection originated from that Eu^{3+} has a stronger affinity towards oxygen-donor components in phosphates than carboxylate groups. Thus, the Pi competes with carboxylate groups to combine with Eu^{3+} and releases them from the surface of CNDs, leading to the disassociation of aggregated CNDs and the recovery of luminescence.

Similarly, the "off-on" fluorescent probe strategy has also been reported with various CNDs precursors and synthesis routes in the determination of F^-,[54] Cu^{2+},[89] SeO_3^{2-},[101] etc. In the Eu-CNDs probe with superior F^- detection performance, the added Eu^{3+} also bound with the carboxylate groups on the surface of CNDs and caused the switch-off of the fluorescence from CNDs. Evidence proved that the quenching process was ascribed to the energy transfer from CNDs to Eu^{3+} (see the second section, Fig. 3B) as well as the aggregation of CNDs (Fig. 3C). Thereafter, the F^- releases Eu^{3+} from CNDs *via* the formation of EuF_3 and turn on the

luminescence again (switch-on). This kind of Eu-CNDs fluorescent probes are highly sensitive, simple and cost-effective, opening new perspectives for the design and development of fluorescent probes with less sophistication, high processibility and better detection accuracy.

An effective way to further improve the sensitivity and stability of the fluorescent probes is to incorporate them into a matrix, such as coating CNDs with polymer, embedding CNDs into metal-organic frameworks (MOFs) and incorporating CNDs with silica nanoparticles, which inspired the design of RE-CNDs.[45] The CNDs imbedded Eu-MOFs (CNDs/Eu-DPA MOFs, DPA–2,6-pyridinedicarboxylic acid) were synthesized for the detection of Cu^{2+}.[114] The MOFs not only shows high stability in water but also have porous nanostructures and high specific surface areas, which facilitate the contact between Cu^{2+} and recognizer to achieve higher sensitivity. Under the excitation of 275 nm, the CNDs/Eu-DPA MOFs emitted dual-luminescence from Eu^{3+} and CNDs. The added Cu^{2+} combined with DPA – the coordinated molecules of Eu^{3+} – and quenched the luminescence of Eu^{3+}, while the emissions from CNDs remained constant. Therefore, a ratiometric fluorescent probe was created with CNDs as the reference and Eu^{3+} as the recognition part, and the ratio of their luminescence intensity F_{425}/F_{615} had a good linear relationship versus the concentration of Cu^{2+} in the range of 0.05-10 μM. By a similar strategy, a CNDs doped Eu-MOFs (CNDs/Eu-MOFs) was reported to have high sensitivity for the determination of Cr^{6+},[116] $NaYF_4$:Yb,Tm@CNDs nanocomposite was used in the detection of Cu^{2+} [120] and $NaYF_4$:Eu@CNDs acted as the sensor for Fe^{3+}.[122] It is anticipated that a similar strategy is applicable to RE-CNDs with other matrixes for higher sensitive and more stable ionic sensing.

Among other ions, Hg^{2+} has drawn tremendous attention due to the high toxicity to public health and the environment. CNDs have already been used for the selective detection of Hg^{2+} in aqueous medium and live cells, because Hg^{2+} shows great affinity towards the carboxylic groups on CNDs, which effectively quenches the CNDs fluorescence with the K_{sv} up to ~1.4×10^7 M^{-1}.[150-152] Based on this, many RE-CNDs fluorescent probes have been designed as developed ratiometric fluorophores for Hg^{2+} detection by the introduction of Eu^{3+} as reference.[92, 153] Xu and co-workers encapsulated CNDs and Eu^{3+} into the MOFs to fabricate the dual-emissive CNDs/Eu@MOFs as a ratiometric and colorimetric fluorescent probe for Hg^{2+} detection.[117] Upon increasing the concentration of Hg^{2+}, the luminescence of CNDs decreased gradually while the emission intensity of Eu^{3+} was well preserved (Fig. 9D and E). As shown in Fig. 9F, the ratio of PL intensities (I_{Eu}/I_{CNDs}) was linearly correlated with the concentration of Hg^{2+} in a wide range of 0-150 μM with the detection limit as low as 13 nM. Importantly, the dual-emissive property endowed the probe with different visualized colour changes from blue to red as the Hg^{2+} increased from 0 to 100 μM (inset photographs in Fig. 9F). Moreover, the CNDs/Eu@MOFs fluorescent probe had better selectivity compared with other metal ions (Fig. 9G). Besides Eu^{3+}, Wu and co-workers designed a CNDs-Tb/APBA () dual-emission probe for the simultaneous detection of NO_2^- and Hg^{2+}.[154] The fluorescent probe had a sensitive response on both ions, based on the specific response of CNDs-Tb and APBA on NO_2^- and Hg^{2+} with different response wavelengths, respectively.

Another application of the RE-CNDs based fluorescent probes is in the detection of water. The most conventional method for water detection is Karl Fischer titration, however, it often suffers from the requirements of specific instruments and sophisticated operational process.[155] In comparison, the RE-CNDs fluorescent probes are highly promising for their fairly simple procedure, low-cost and fast response rate. The sensing of water by RE-CNDs is based on the different luminescent performances in organic and aqueous solvents due to the various dispersion status of CNDs. Dong and co-workers reported a water sensor based on the Eu^{3+}-MOFs incorporated with nitrogen and sulfate co-doped CNDs (N,S-CNDs), referred to as N, S-CNDs/Eu-MOFs.[115] The N, S-CNDs/Eu-MOFs had both the red emission of Eu^{3+} and the blue emission of CNDs. In organic solvents (i.e. ethanol, N, N-dimethylformamide (DMF) and acetonitrile), the CNDs aggregate and are limited in the chambers of Eu-MOFs, thus only the red luminescence from Eu^{3+} is detectable. After dispersed in aqueous solution, the encapsulated CNDs were released from the frameworks and recovered PL, while the luminescence of Eu^{3+} was quenched by the O-H vibrations in water (Fig. 10A). Therefore, the N, S-CNDs/Eu-MOFs was a good colorimetric sensor that the PL colour changed from visible red to blue gradually with the increase of water content in ethanol in a wide response range of 0.2-30% (V/V) (Fig. 10B). The PL spectra of the sensing process are shown in Fig. 10C and D. Another work of water sensing was reported by Wu *et al.*.[118] After synthesizing a red-emitting CNDs-doped MOFs *via* a one-step hydrothermal method and then introducing green-emitting Tb^{3+} into it, a dual emissive CNDs/Tb@MOFs was prepared. Different from the sensor mentioned above, the CNDs in CNDs/Tb@MOFs are well dispersed in organic solvents (ethanol, DMF and cyclopropane) but aggregated in water, with the PL emission colours varied from red to green when the water content increased (Fig. 10E). The ratio of the PL intensity I_{545}/I_{605} had a good linear correlation with water content in the range of 0-30% (V/V). These applications open up new possibilities for the design of RE-CNDs fluorescent probes with more simple procedure, higher visualization and better sensitivity in the field of water detection.

4.2.3. Temperature and pH sensing. Inspiring from their excellent fluorescent properties, RE-CNDs are also utilized as optical probes in the temperature and pH sensing.[121, 123] Conventional methods for temperature monitoring are based on the detection of heat flow from the invasive probes, which often suffer from limited accuracy and resolution, especially in small confined spaces. To address this problem, fluorescence-based measurements are emerging which exhibit more desired advantages with noninvasive detection and high stability.[156, 157] The group of Lei reported a ratiometric temperature sensor based on dual-emissive

CNDs/Al_2O_3:Eu^{3+}, where both the fluorescence of Eu^{3+} (λ_{em} = 616 nm) and CNDs (λ_{em} = 425 nm) are weakened as the temperature increases.[123] The ratio of these two emission peaks F_{616}/F_{425} showed a linear relationship with temperature in the range of 100-360 K. Besides, the pH responsiveness was reported by Zhang *et al*., where dual-emissive Eu-CNDs showed ratiometric pH sensing.[88] Notably, CNDs has already been widely used in temperature and pH sensing, whereas the development of dual-emissive RE-CNDs sensors provides a self-calibration function by measuring the ratio of fluorescent intensity without the disturbance from the background. These researches are good examples for further design of RE-CNDs in versatile sensing.

4.3. Other applications

4.3.1. Anti-counterfeiting. Fluorescent anti-counterfeiting and authentication technologies are attracting increasing attention due to their facile manipulation and rapid responsivity under UV irradiation.[158-164] RE-CNDs based materials are one of the most promising candidates using as security materials, which are invisible under sunlight while possessing photo-switchable fluorescence upon UV irradiation. Firstly, they can be designed for anti-counterfeiting films.[164, 165] As reported by Li *et al.*, the synthesized CNDs-Eu nanorods were incorporated into an electrospun nanofibrous membrane with PVA (poly(vinylalcohol)).[164] The prepared membrane was white under sunlight and red under UV-light excitation. Interestingly, the fluorescence of the membrane would tune to blue after finger touching, because the Pi in sweats could bind with Eu^{3+} and blocked the energy transfer from CNDs to Eu^{3+}, making this intelligent material quite promising for finger and document security. Besides, RE-CNDs are excellent components for anti-counterfeiting inks. Wang *et al.* fabricated a kind of luminescent ink by mixing CNDs with the RE complexes $Ln(DPA)_3$ (Ln = Eu and Tb).[124, 127] The obtained luminescent inks had UV light-switchable colour images. Through adjusting different mass ratios of $Eu(DPA)_3$ and $Tb(DPA)_3$, the inks performed diverse emission colours from red to green under 254 nm UV excitation and blue under 356 nm UV light. Besides, the CNDs/$NaLuF_4$:Yb,Er microcrystals were reported as anti-counterfeiting inks for the label of the logo, with green UC emission under 980 nm excitation and blue emission under 365 nm excitation. Therefore, the multiple and adjustable luminescent properties, high photo-stability and superior hydrophilicity of RE-CNDs endow them with great potential in fabricating luminescent tags and labels for security concern, which desire further exploration for other anti-counterfeiting applications.

4.2.3. Bioimaging. Since reported by Sun *et al.* in 2006,[166] CNDs have been successfully used in bioimaging owing to their high photostability, bright fluorescence at the individual level, excellent biocompatibility and cellular uptakes.[167, 168] RE-CNDs combine both the merits from CNDs and the versatile luminescence of RE^{3+}, which considerably extend their applications in cellular and *in vivo* imaging. For example, through the introduction of Yb^{3+} or Nd^{3+}, the RE-CNDs had not only the blue emission from CNDs but also the characteristic emissions in the NIR region from Yb^{3+} or Nd^{3+} centred at 998 nm and 1068 nm, respectively.[90] This provides new ideas for the development of RE-CNDs with NIR response, following the current trend in high-quality bioimaging with deep penetration, high resolution and negligible tissue scattering. Besides, RE-CNDs have also been used in Hela cell imaging with UC/DC emissions,[120] fungal imaging,[92] and other cell imaging applications.[153] There's no doubt that RE-CNDs are excellent probes for optical bioimaging with great expansibility and designability in the biomedical field in the future.

5. Applications of Multifunctional Magnetic-Optical RE-CNDs

5.1. Multi-modal imaging probes based on Gd-CNDs or Gd/Yb-CNDs

Among plenty of imaging techniques, MRI, CT, fluorescence imaging (FI), ultrasound imaging (USI) and PET have been widely used in clinical diagnosis and therapeutics. Each of them has its own unique advantages and inherent limitations such as the limited penetration depth, sensitivity and resolution. Thus, the single imaging mode cannot fully meet all the requirements and demands in clinical diagnosis. To overcome this challenge, integrating multi imaging techniques into a single system realize the complementary effect, improve the imaging quality, and provide more precise information. Hybrid nanomaterials have drawn tremendous attention for multiple biomedical applications in recent years due to superior performances in multi-mode imaging, diagnostic and therapeutic integrated platforms. By virtue of the excellent MRI property of Gd^{3+} and the excellent fluorescent property of hydrophilic CNDs, the Gd-CNDs are highly desirable dual-modal imaging platform to afford both high r_1 relaxivity and strong photo-fluorescence. Therefore, Gd-CNDs combine both the high fluorescent sensitivity as well as excellent spatial and temporal resolutions of MRI, which cannot be achieved by individual components.

Gd-CNDs with dual-modal imaging have been successfully fabricated from various precursors, mostly *via* simple treatment processes. The group of Chen fabricated Gd imbedded CNDs (Gd-CNDs) by a direct calcination of the Gd-DTPA - a conventional MRI contrast agent, where Gd-DTPA acted as the source of both Gd^{3+} and CNDs.[138] Gd-CNDs present both high longitudinal relaxivity (r_1) of 5.88 mM^{-1} s^{-1} (significantly higher than Gd-DTPA, 3.10 mM^{-1} s^{-1})[169] and intensive PL from CNDs, supporting their great potential as MRI-fluorescence dual-modal imaging probes.

From another point of view, the inert CNDs shell not only suppresses the leakage of Gd^{3+} but also render Gd-CNDs good hydrophilicity and colloidal stability, which is attributed to the abundant functional groups on the surface of CNDs. More importantly, the unique surface environments also contributed to the efficient renal clearance of Gd-CNDs and their conjugates in biological systems. One major issue faced by inorganic nanoparticles used in biomedical applications is the long-term toxicity. Previous research by Frangioni's group proved that nanoparticles can be excreted by the kidney with the hydrodynamic diameter around 5.5 nm and the zwitterionic surface charge.[170] Although the size requirement is hard to fulfill by Gd-based contrast agents, there is an intriguing result that the Gd-CNDs and their conjugates can be effectively cleared through the urine with a size of 12 nm, which is above the threshold for renal clearance. After 4 h of the intravenous injection (0.8 mg Gd/kg), the signals in most of the organs in the T_1-weighted images recovered to the pre-injection levels (Fig. 11A). Meanwhile, greatly enhanced signals were observed in the bladder, which proved the urine clearance (Fig. 11B). The PL spectra of the urine samples are shown in Fig. 11C. The author stressed the important role of surface groups on CNDs, which imparted Gd-CNDs with great colloidal stability and help them cross the biological barriers, especially the carboxylic groups. This verified the significance of the unique surface modification on CNDs for *in vivo* clearance.[171]

Owing to the modifiable surface of CNDs, the Gd-CNDs are further conjugated with target-specific biomolecules to obtain advanced function. For example, the above-synthesized Gd-CNDs were functionalized with arginine-glycine-aspartic acid (RGD) tripeptide as RGD-Gd-CNDs. The RGD is a tumour-targeting peptide with a strong affinity towards integrin $\alpha_v\beta_3$ overexpressed cancer cells, which impart RGD-Gd-CNDs with the ability of targeted identification and imaging for U87MG tumor.[172] The RGD-Gd-CNDs are uptaken by cells *via* RGD-integrin interaction and concentrated in endosomes/lysosomes of cells.[129, 138] In the T_1-weighted coronal MR images shown in Fig. 11D and E, the MRI signals in tumours of animals enhanced by 42.6 ± 0.08% after injection of RGD-Gd-CNDs when compared to those with the injection of Gd-CNDs. Other biomolecules like the anti-EGFR affibodies - EGFR (Epidermal growth factor receptor) is a tumour biomarker overexpressed in many human tumours - were modified to the Gd-CNDs using for tumour-targeted imaging.[141]

Afterward, different one-step procedures for the synthesis of Gd-CNDs were conducted and reported. Xu and co-workers prepared Gd-CNDs hybrid nanoprobe *via* a one-pot hydrothermal process.[129] The synthesized Gd-CNDs have a better MRI response (r_1 = 7.36 mM^{-1} s^{-1}) when compared with Gd-DTPA while maintaining the fluorescence of CNDs simultaneously. The dual-modal imaging was verified through the zebrafish embryo and mice models (Fig. 11F and G). The Gd-CNDs fabricated by Chen *et al.* not only promote the proliferation of human Mesenchymal stem cells (hMSCs) but also monitor the multiplication process at the cellular level by the fluorescence of the material.[133] The superior MRI quality of Gd-CNDs provided possibilities for the intrinsic tracking of hMSCs. Moreover, Gd-CNDs fabricated by Liao *et al.* through one-step hydrothermal had the r_1 value up to 14.08 mM^{-1} s^{-1}.[131] Other synthetic routes like one-step pyrolysis [173] and microwave-assisted polyol method were also developed in the fabrication of Gd-CNDs.[130] These methods are usually based on facile steps and easily-obtained precursors, improving the synthesis strategy for practical MRI/fluorescence bimodal imaging probes.

With the aid of ligands, the synthesis of Gd-based CNDs is also achieved in the form of Gd-DTPA-CNDs, as described in section 3. Shi and co-workers chelated Gd^{3+} onto the outer surface of DTPA-functionalized CNDs, where the Gd-DTPA-CNDs had dramatically improved longitudinal relaxivity (r_1 = 56.72 mM^{-1} s^{-1}).[86] This design idea is based on the different influence of Gd^{3+} on neighbouring water molecules, where the outer Gd^{3+} has a greater effect on the longitudinal relaxivity of water than the Gd^{3+} in the core of nanoparticles. Besides, Gd-DTPA-CNDs had excellent fluorescent imaging performance alongside with great water solubility and negligible cytotoxicity.

Despite the prominent properties of MRI/fluorescence dual-mode probe, Gd-CNDs still have limitations when it comes to hypointense regions, such as calculus, calcification and cortical bone. To address this drawback and further extend the versatility of RE-CNDs imaging platforms, Gd^{3+} and Yb^{3+} are co-doped into CNDs to achieve MRI/CT/fluorescence multimodal imaging. Yb-contained nanomaterials have been ideal alternatives applied as CT contrast agents due to their stronger X-ray attenuation coefficient than that of the commercial iodine-based X-ray contrast agents (Yb 3.88 cm^2/g; I, 1.94 cm^2/g at 100 eV).[174, 175] Zhao *et al.* fabricated the first example of Gd/Yb-CNDs through a one-step hydrothermal process. The Gd/Yb-CNDs imaging platform not only showed superior photostability, high longitudinal relaxivity (r_1 = 6.65 mM^{-1} s^{-1}) and excellent X-ray absorption (45.43 HU L g^{-1}), but also exhibited great renal elimination. Fig. 11H-K showed the concentration-dependent enhancement of the MRI and CT signal intensity with the increasing concentrations of Gd^{3+} and Yb^{3+}, respectively. Notably, the r_1 of Gd/Yb-CNDs was higher than that of the clinical Gd-DTPA (r_1 = 3.69 mM^{-1} s^{-1}) (Fig. 11H and I). Moreover, the contrast intensity of the CT images in Gd/Yb-CNDs was stronger than the commercial iobitridol under the same concentrations (Fig. 11J and K). Similar multimodal contrast agent N/Gd/Yb-CNDs was reported by the group of Fernandez, which performed excellent fluorescence, MRI and CT imaging capabilities. The co-doped CNDs had superior fluorescent intensity with high quantum yield (66 ± 7%) and negligible cytotoxicity after the exposure to different cell lines (24 h and 72 h incubation). This is efficient for the *in vitro* cell fluorescent imaging along with the *in vitro* and *in vivo* MR and CT imaging. The abovementioned Gd/Yb-CNDs provided a kind of novel multimodal imaging platform by

a simple synthesis approach to realize long-term *in vivo* stability and valuable MR/CT/fluorescence contrast performances. Along with their great excretion through the renal elimination pathway, Gd/Yb-CNDs is a promising nanoprobe for biomedical research and clinical applications. Most notably, this nanomaterial can be further modified with particular biomarkers to obtain imaging-guided targeting, which is achieved through anchoring appropriate moieties onto the surface of CNDs. This provides new ideas for further improving and optimizing the functionality of Gd/Yb-doped CNDs, inspiring more explorations in the near future.

It is well known that the superparamagnetic Fe_3O_4 nanoparticles are great T_2-weighted contrast agents. Thus, integrating Gd^{3+} and Fe_3O_4 into a single particle simultaneously realizes the MRI with both the T_1 and T_2 imaging ability. Huang *et al.* prepared a dual-modal imaging probe Gd-CNDs@Fe_3O_4 through covalent binding Gd-CNDs with the amino-functionalized Fe_3O_4.[132] Nevertheless, there are still limited reports on Gd-CNDs based T_1 and T_2 integrated contrast agents, which require more explorations in case of the improvement of imaging accuracy and detection quality.

5.2. Theranostic platform based on Gd-CNDs

In the modern world, environment and energy problems are two of the greatest issues in human society to be addressed. As to the medical field, many efforts have been focusing on high effective multiple treatment strategies in clinical use, including prevention, diagnosis, and therapy.[44] The concept "theranostics" thus has been introduced to create a single platform combining both the diagnostics and therapeutics.[33] The theranostics not only provides a non-invasive strategy for the assessment and visualization of drug distribution *in vivo* but also realizes the monitoring of real-time therapeutic responses.[176] Especially in radiotherapy, theranostics addresses the two limitations of precise localization and sensitivity towards tumors.[177]

The theranostics based on MRI is attracting increasing interests recently, which combines the molecule diagnosis and therapy in the treatment of diseases. Among other agents for theranostics, Gd-based nanomaterials are the most useful ones because they offer a single platform with enhanced signal intensity and prolonged *in vivo* imaging time. Owing to the high atomic number (Z = 64), Gd possesses a high X-ray photon capture cross-section and Compton scattering effect, which contributes to the decreased radiation dose and less damage to normal tissues.[178] The Gd-CNDs prepared by Du *et al*. showed increased inhibition on tumor growth in the radiotherapy through a radiosensitizing effect, in contrast to the treatment of X-ray irradiation alone.[139] This kind of Gd-CNDs based ultra-small rigid platform provides precise localization for MRI-guided radiotherapy and accurate anatomical and pathophysiological information, as well as realizes enhanced radiosensitization, indicating their great potential in the integrated diagnosis and therapy for clinical applications in the future.

6. Conclusions and Perspectives

With scientific advances, the development of interdisciplinary technology and hybrid materials are of great interest. RE-CNDs is a kind of brand-new hybrid nanomaterial extending the multifunctional applications of single component RE materials by combining the merits of unique optical properties and the modifiable functional surface of CNDs. In conclusion, this review provides a comprehensive summary of recent reports on RE-CNDs, discussed the mechanism and structure-to-function synthesis strategies of luminescent and magnetic-optical multimodal RE-CNDs, and finally reviewed their applications in respect to the biomedical field. The applications of RE-CNDs hybrid nanomaterials are mainly concentrated on their luminescent and magnetic properties. On one hand, the excellent PL, hydrophilicity and photostability of CNDs, combining with the superior optical properties of RE, bestow RE-CNDs great advantages in multi-modal fluorescence, bioanalysis and biosensing, etc. Notably, the energy transfer processes between CNDs and RE^{3+} are elucidated, which play an important role in the luminescent and bioanalytical applications of RE-CNDs. From another point of view, the Gd-CNDs based multi-modal magnetic-optical imaging platforms have excellent performance owing to their ultra-small sizes, improved relaxivity, great biocompatibility and surface modifiability compared with traditional Gd-complex based MRI contrast agents, showing great promise in multi-modal MRI bioimaging and theranostics in the future.

Despite a variety of research work considering RE-CNDs hybrid nanomaterials published in recent years, there are still great challenges and obstacles for practical and advanced applications. Most importantly, the research on the energy transfer and interaction mechanisms of luminescent RE-CNDs is still at the primary stage. Although lots of evidence have proven the energy transfer process between CNDs and Eu^{3+}/Tb^{3+}, there is still a lack of deep explorations and quantitative studies about this field. The unclear mechanism hinders the controllable modulation of the energy transfer process through the design and fabrication of RE-CNDs. Therefore, more valuable research to provide concrete proofs of the theories are needed in the future. Besides, the abundant functional groups on CNDs provide large modification possibilities, which are of great significance for further multiple design and combination with organic molecules and biomarkers, whereas relative research is still quite rare. What's more, the RE-CNDs hybrids introduced above mainly focus on the field of luminescence, biosensing and bioimaging, and the referred RE^{3+} are limited to a few types.

For the Gd-based CNDs, the preclinical applications of Gd-based CNDs have been hindered by the systematic *in vivo* risk assessment, especially for the relative immunotoxicity, which leads to the bottleneck of further development of the modulations in sizes, shapes, and compositions.[179-181] As mentioned in section 2.2.2., the NSF is potential to be induced by the Gd-based complexes in patients with kidney dysfunction. Besides the Gd ions, the concerns for the safety of CNDs materials in the human body also prevents the clinic applications. Although animal studies have confirmed that no toxic evidence of carbon materials to mice, the accumulation and stay of carbon nanotubes or graphene in the main organs still raises strong concerns about toxicity tolerance.[182, 183] Thus, appropriate and comprehensive evaluations of the relative immunotoxicity of Gd-based CNDs are critical to analyze their potential for clinic applications and provides rational suggestions for the future design of non-immunotoxic RE based agents. Meanwhile, the short *in vivo* circulation lifetime of Gd-based CNDs is another key shortcoming, which results in the high cost and low contrast efficiency.

Therefore, it is of great urgency to explore more design and application possibilities. In this sense, this review provides a reference for further research in a wider aspect of the RE-CNDs hybrid nanomaterials other than the abovementioned application fields. To enable the expansion of RE-CNDs to wider fields, we outline several opportunities for future development on interdisciplinary research, involving biomedicine, tissue engineering, energy, catalysis, etc.

(1) Exploration of new multifunctional RE-CNDs. According to the trend of development, the hybrids are promising materials in chemical and biomedical areas. Owing to the versatile properties of RE^{3+} and the abundant surface groups on CNDs, the performance and multifunctionality of RE-CNDs can be further improved through tailoring the precursors and synthesis procedures, doping with other biomolecules and compositing with various organic/inorganic matrixes. For example, except for the visible-emitting RE^{3+} (e.g. Eu^{3+} and Tb^{3+}), other RE^{3+} with NIR emissions, UC luminescence, and the long afterglow luminescence can also combine with CNDs. These materials have great potential in the treatment of critical diseases, such as high precision targeted therapy, multifunctional integrated diagnosis and treatment platform, and even the diagnosis and treatment of the Corona Virus Disease 2019 (COVID-19). Moreover, doping Ce^{3+}/Ce^{4+} into CNDs takes advantage of both the properties of cerium (anti-oxidation/antibacterial)[184, 185] and the great hydrophilicity and biocompatibility of CNDs, which cannot be achieved by pure CeO_2 nanoparticles.[186] This kind of cerium-based RE-CNDs can be used as an antioxidant-imaging dual-mode platform in the field of nanomedicine, including the novel cancer therapeutics and treatments for Alzheimer's disease (AD).

(2) New strategies for the design of RE-CNDs in energy storage and conversion field. In recent years, due to the unique quantum confinement effects and surface defects, CNDs have been proven to have excellent performance in the field of energy storage and conversions, such as electro- and photo-catalysis, light-emitting diodes (LED), supercapacitors and lithium/sodium ion batteries.[8] CNDs possess both excellent optical and electronic properties, and their energy levels and gaps can be tuned through controlling the size, crystallinity, functional groups and heteroatoms doping. Combining the RE^{3+} with abundant electron levels and superior advantages in the field of solar-energy conversion, rechargeable hydride batteries, electronics, economical lighting and so forth, RE-CNDs are promising candidates in energy-related areas, which worth further exploration in the future.

In summary, the development of RE-CNDs hybrids is still in its infancy. Current research has proven the successful applications of RE-CNDs in luminescence, biosensing and bioimaging field. However, how to improve the fluorescent efficiency, acquire higher sensitivity in sensing and better resolution in bioimaging are core issues to be solved in the near future. We firmly believe that this review will provide novel ideas from the design to the multiple subsequent applications of RE-CNDs, which will inspire more scientists to the development of this new material in both fundamental research and industrial applications, thus benefits the scientific community to solve the urgent challenges ranging from biomedical diagnosis to the global energy crisis in the future.

Conflicts of interest

There are no conflicts to declare.

Acknowledgements

We gratefully acknowledge the support from the National Key R&D Program of China (2017YFA0208000), the Fundamental Research Funds for the Central Universities, Nankai University (63201071 and ZB19500202), National Natural Science Foundation of China (21971117 and 21771156), State Key Laboratory of Rare Earth Resource Utilization (RERU2019001) and the 111 Project (B18030) from China.

Notes and references

1. T. Cheisson and E. J. Schelter, *science*, 2019, **363**, 489-493.
2. Z.-G. Yan and C.-H. Yan, *journal of materials chemistry*, 2008, **18**, 5046-5059.
3. S. V. Eliseeva and J.-C. G. Bünzli, *new journal of chemistry*, 2011, **35**, 1165-1176.
4. H. Dong, S.-R. Du, X.-Y. Zheng, G.-M. Lyu, L.-D. Sun, L.-D. Li, P.-Z. Zhang, C. Zhang and C.-H. Yan, *Chemical Reviews*, 2015, **115**, 10725-10815.
5. P. Roy, P.-C. Chen, A. P. Periasamy, Y.-N. Chen and H.-T. Chang, *materials today*, 2015, **18**, 447-458.
6. S. Zhu, Y. Song, X. Zhao, J. Shao, J. Zhang and B. Yang, *nano research*, 2015, **8**, 355-381.
7. S. N. Baker and G. A. Baker, *angewandte chemie*, 2010, **49**, 6726-6744.
8. C. Hu, M. Li, J. Qiu and Y.-P. Sun, *chemical society reviews*, 2019, **48**, 2315-2337.
9. W. Liu, C. Li, Y. Ren, X. Sun, W. Pan, Y. Li, J. Wang and W. Wang, *journal of materials chemistry b*, 2016, **4**, 5772-5788.
10. Y. Park, J. Yoo, B. Lim, W. Kwon and S. W. Rhee, *journal of materials chemistry*, 2016, **4**, 11582-11603.
11. H. Liu, L. Zhang, M. Yan and J. Yu, *journal of materials chemistry b*, 2017, **5**, 6437-6450.
12. V. Sharma, P. Tiwari and S. M. Mobin, *journal of materials chemistry b*, 2017, **5**, 8904-8924.
13. S.-T. Yang, L. Cao, P. G. Luo, F. Lu, X. Wang, H. Wang, M. J. Meziani, Y. Liu, G. Qi and Y.-P. Sun, *Journal of the American Chemical Society*, 2009, **131**, 11308-11309.
14. S. Augustine, J. Singh, M. Srivastava, M. Sharma, A. Das and B. D. Malhotra, *biomaterials science*, 2017, **5**, 901-952.
15. K. Nekoueian, M. Amiri, M. Sillanpää, F. Marken, R. Boukherroub and S. Szunerits, *chemical society reviews*, 2019, **48**, 4281-4316.
16. Y. Chen, Y. Cao, C. Ma and J.-J. Zhu, *materials chemistry frontiers*, 2020, **4**, 369-385.
17. S. Comby and T. Gunnlaugsson, *ACS Nano*, 2011, **5**, 7184-7197.
18. B. Wang, J. Hai, Q. Wang, T. Li and Z. Yang, 2011, **50**, 3063-3066.
19. W. Sun, J. Yu, R. Deng, Y. Rong, B. Fujimoto, C. Wu, H. Zhang and D. T. Chiu, *Angewandte Chemie-International Edition*, 2013, **52**, 11294-11297.
20. L. J. Charbonniere, N. Hildebrandt, R. F. Ziessel and H.-G. Lohmannsroben, *journal of the american chemical society*, 2006, **128**, 12800-12809.
21. L. Fu, Z. Liu, Y. Liu, B. Han, J. Wang, P. Hu, L. Cao and D. Zhu, *advanced materials*, 2004, **16**, 350-352.
22. S. Kyatskaya, J. R. G. Mascarós, L. Bogani, F. Hennrich, M. Kappes, W. Wernsdorfer and M. Ruben, *journal of the american chemical society*, 2009, **131**, 15143-15151.
23. K.-T. Yong, W.-C. Law, R. Hu, L. Ye, L. Liu, M. T. Swihart and P. N. Prasad, *Chemical Society Reviews*, 2013, **42**, 1236-1250.
24. 31, 2007.
25. A. M. Alex, M. D. Kiran, G. Hari, A. Krishnan, J. S. Jayan and A. Saritha, *materials today proceedings*, 2020, DOI: 10.1016/J.MATPR.2019.12.409.
26. L. Cao, X. Wang, M. J. Meziani, F. Lu, H. Wang, P. G. Luo, Y. Lin, B. A. Harruff, L. M. Veca and D. Murray, *Journal of the American Chemical Society*, 2007, **129**, 11318-11319.
27. K. Binnemans, *chemical reviews*, 2009, **109**, 4283-4374.
28. L. Pan, S. Sun, A. Zhang, K. Jiang, L. Zhang, C. Dong, Q. Huang, A. Wu and H. Lin, *Adv. Mater.*, 2015, **27**, 7782-7787.
29. Y. Chen, M. Zheng, Y. Xiao, H. Dong, H. Zhang, J. Zhuang, H. Hu, B. Lei and Y. Liu, *Adv. Mater.*, 2016, **28**, 312-318.
30. L. Wang, S. J. Zhu, H. Y. Wang, S. N. Qu, Y. L. Zhang, J. H. Zhang, Q. D. Chen, H. L. Xu, W. Han, B. Yang and H. B. Sun, *ACS Nano*, 2014, **8**, 2541-2547.
31. A. B. Bourlinos, A. Bakandritsos, A. Kouloumpis, D. Gournis, M. Krysmann, E. P. Giannelis, K. Polakova, K. Safarova, K. Hola and R. Zboril, *J. Mater. Chem.*, 2012, **22**.
32. W. A. High, R. A. Ayers, J. Chandler, G. Zito and S. E. Cowper, *journal of the american academy of dermatology*, 2007, **56**, 21-26.
33. Y. Liu and N. Zhang, *biomaterials*, 2012, **33**, 5363-5375.
34. Y. Liu, K. Ai, Q. Yuan and L. Lu, *biomaterials*, 2011, **32**, 1185-1192.
35. H. Yang, S. Santra, G. A. Walter and P. H. Holloway, *advanced materials*, 2006, **18**, 2890-2894.
36. J. L. Vivero-Escoto, W. J. Rieter, H. Lau, R. C. Huxford-Phillips and W. Lin, *small*, 2013, **9**, 3523-3531.
37. I. X. Cantarelli, M. Pedroni, F. Piccinelli, P. Marzola, F. Boschi, G. Conti, A. Sbarbati, P. Bernardi, E. Mosconi, L. Perbellini, L. Marongiu, M. Donini, S. Dusi, L. Sorace, C. Innocenti, E. Fantechi, C. Sangregorio and A. Speghini, *biomaterials science*, 2014, **2**, 1158-1171.
38. Z. Zhou, D. Huang, J. Bao, Q. Chen, G. Liu, Z. Chen, X. Chen and J. Gao, *advanced materials*, 2012, **24**, 6223-6228.
39. C. C. Huang, C. H. Su, W. M. Li, T. Y. Liu, J. H. Chen and C. S. Yeh, *advanced functional materials*, 2009, **19**, 249-258.
40. J.-L. Bridot, A.-C. Faure, S. Laurent, C. Rivière, C. Billotey, B. Hiba, M. Janier, V. Josserand, J.-L. Coll, L. V. Elst, R. Muller, S. Roux, P. Perriat and O. Tillement, *journal of the american chemical society*, 2007, **129**, 5076-5084.
41. G. Liu and B. Jacquier, *Spectroscopic properties of rare earths in optical materials*, 2005.
42. J.-C. G. Bünzli, *chemical reviews*, 2010, **110**, 2729-2755.
43. S. V. Eliseeva and J.-C. G. Bünzli, *chemical society reviews*, 2010, **39**, 189-227.
44. L. Prodi, E. Rampazzo, F. Rastrelli, A. Speghini and N. Zaccheroni, *chemical society reviews*, 2015, **44**, 4922-4952.
45. S. Y. Lim, W. Shen and Z. Gao, *chemical society reviews*, 2015, **44**, 362-381.
46. A. P. Demchenko and M. O. Dekaliuk, *methods and applications in fluorescence*, 2013, **1**.
47. S. I. Weissman, *journal of chemical physics*, 1942, **10**, 214-217.
48. X. Wang, L. Cao, F. Lu, M. J. Meziani, H. Li, G. Qi, B. Zhou, B. A. Harruff, F. Kermarrec and Y.-P. Sun, *chemical communications*, 2009, DOI: 10.1039/B906252A, 3774-3776.
49. L. Armelao, S. Quici, F. Barigelletti, G. Accorsi, G. Bottaro, M. Cavazzini and E. Tondello, *coordination chemistry reviews*, 2010, **254**, 487-505.

50. J.-C. G. Bünzli, *coordination chemistry reviews*, 2015, **293**, 19-47.
51. H. X. Zhao, L. Q. Liu, Z. D. Liu, Y. Wang, X. J. Zhao and C. Z. Huang, *chemical communications*, 2011, **47**, 2604-2606.
52. T. Ji, P. Fan, X. Li, Z. Mei, Y. Mao and Y. Tian, *rsc advances*, 2019, **9**, 10645-10650.
53. T. D.-F. López, A. F. González, M. E. Díaz-García and R. Badía-Laíño, *carbon*, 2015, **94**, 142-151.
54. P. Singhal, B. G. Vats, S. K. Jha and S. Neogy, *acs applied materials & interfaces*, 2017, **9**, 20536-20544.
55. H. Dong, A. Kuzmanoski, D. M. Gößl, R. Popescu, D. Gerthsen and C. Feldmann, *chemical communications*, 2014, **50**, 7503-7506.
56. T. Förster, *annalen der physik*, 1948, **437**, 55-75.
57. H. Sahoo, *journal of photochemistry and photobiology c photochemistry reviews*, 2011, **12**, 20-30.
58. Y. Haas and G. Stein, *the journal of physical chemistry*, 1971, **75**, 3668-3677.
59. X. Xu, X. Zhang, C. Hu, Y. Zheng, B. Lei, Y. Liu and J. Zhuang, *journal of materials chemistry c*, 2019, **7**, 6231-6235.
60. Y. Wang, F. Hong, L. Yu, H. Xu, G. Liu, X. Dong, W. Yu and J. Wang, *journal of luminescence*, 2020, **221**.
61. T. Samanta, C. Hazra and V. Mahalingam, *new journal of chemistry*, 2015, **39**, 106-109.
62. Q. Huo, W. Tu and L. Guo, *optical materials*, 2017, **72**, 305-312.
63. J. Huang, B. Tian, J. Wang, Y. Wang, W. Lu, Q. Li, L. Jin, C. Li and Z. Wang, *crystengcomm*, 2018, **20**, 608-614.
64. J. Huang, W. Lu, J. Wang, Q. Li, B. Tian, C. Li, Z. Wang, L. Jin and J. Hao, *inorganic chemistry*, 2018, **57**, 8662-8672.
65. J. R. Lakowicz and B. R. Masters, *journal of biomedical optics*, 2008, **13**, 29901.
66. P. Verwilst, S. Park, B. Yoon and J. S. Kim, *chemical society reviews*, 2015, **44**, 1791-1806.
67. S. Biju, J. Gallo, M. Bañobre-López, B. B. Manshian, S. J. Soenen, U. Himmelreich, L. V. Elst and T. N. Parac-Vogt, *chemistry a european journal*, 2018, **24**, 7388-7397.
68. J. Key and J. F. Leary, *international journal of nanomedicine*, 2014, **9**, 711-726.
69. D. E. Lee, H. Koo, I. C. Sun, J. H. Ryu, K. Kim and I. C. Kwon, *chemical society reviews*, 2012, **41**, 2656-2672.
70. L. Zhang, J. Li and K. Liu, *science china technological sciences*, 2018, **61**, 1329-1333.
71. P. Mi, D. Kokuryo, H. Cabral, H. Wu, Y. Terada, T. Saga, I. Aoki, N. Nishiyama and K. Kataoka, *nature nanotechnology*, 2016, **11**, 724-730.
72. N. Lee and T. Hyeon, *chemical society reviews*, 2012, **41**, 2575-2589.
73. A. M. Funk, V. C. Jordan, A. D. Sherry, S. J. Ratnakar and Z. Kovacs, *angewandte chemie*, 2016, **55**, 5024-5027.
74. L. M. Manus, D. J. Mastarone, E. A. Waters, X. Q. Zhang, E. A. Schultz-Sikma, K. W. MacRenaris, D. Ho and T. J. Meade, *nano letters*, 2010, **10**, 484-489.
75. H. B. Na and T. Hyeon, *journal of materials chemistry*, 2009, **19**, 6267-6273.
76. C. Cabella, S. G. Crich, D. Corpillo, A. Barge, C. Ghirelli, E. Bruno, V. Lorusso, F. Uggeri and S. Aime, *contrast media & molecular imaging*, 2006, **1**, 23-29.
77. M. R. Prince, H. L. Zhang, G. H. Roditi, T. Leiner and W. Kucharczyk, *journal of magnetic resonance imaging*, 2009, **30**, 1298-1308.
78. K. N. Raymond and V. C. Pierre, *bioconjugate chemistry*, 2005, **16**, 3-8.
79. N. Feliu, D. Docter, M. Heine, P. d. Pino, S. Ashraf, J. Kolosnjaj-Tabi, P. Macchiarini, P. Nielsen, D. Alloyeau, F. Gazeau, R. H. Stauber and W. J. Parak, *chemical society reviews*, 2016, **45**, 2440-2457.
80. R. B. Lauffer, *chemical reviews*, 1987, **87**, 901-927.
81. S. Aime, M. Botta and E. Terreno, *advances in inorganic chemistry*, 2005, **57**, 173-237.
82. P. Caravan, J. J. Ellison, T. J. McMurry and R. B. Lauffer, *chemical reviews*, 1999, **99**, 2293-2352.
83. N. J. J. Johnson, W. Oakden, G. J. Stanisz, R. S. Prosser and F. C. J. M. v. Veggel, *chemistry of materials*, 2011, **23**, 3714-3722.
84. Y. Tian, H.-Y. Yang, K. Li and X. Jin, *journal of materials chemistry*, 2012, **22**, 22510-22516.
85. G. H. Lee, E. S. Choi, J. Y. Park, K. Kattel, W. Xu, M. J. Baek, J. H. Kim, Y. Chang and T. J. Kim, *journal of the korean physical society*, 2010, **56**, 1532-1536.
86. Y. Shi, Y. Pan, J. Zhong, J. Yang, J. Zheng, J. Cheng, R. Song and C. Yi, *carbon*, 2015, **93**, 742-750.
87. Y. Zhao, X. Hao, W. Lu, R. Wang, X. Shan, Q. Chen, G. Sun and J. Liu, *Journal*, 2018, **1**, 2544-2551.
88. T. Zhang, Y. Zhai, H. Wang, J. Zhu, L. Xu, B. Dong and H. Song, *rsc advances*, 2016, **6**, 61468-61472.
89. Z. Ye, R. Tang, H. Wu, B. Wang, M. Tan and J. Yuan, *new journal of chemistry*, 2014, **38**, 5721-5726.
90. F. Wu, H. Su, X. Zhu, K. Wang, Z. Zhang and W.-K. Wong, *journal of materials chemistry b*, 2016, **4**, 6366-6372.
91. X. Liu, Z. Xu, C. Chen, D. Tian, L. Yang, X. Luo, A. A. A. Kheraif and J. Lin, *journal of materials chemistry c*, 2019, **7**, 2361-2375.
92. M. L. Desai, S. Jha, H. Basu, R. K. Singhal, P. K. Sharma and S. K. Kailasa, *new journal of chemistry*, 2018, **42**, 6125-6133.
93. B. B. Chen, Z. X. Liu, H. Y. Zou and C. Z. Huang, *analyst*, 2016, **141**, 2676-2681.
94. M. Rong, X. Deng, S. Chi, L. Huang, Y. Zhou, Y. Shen and X. Chen, *mikrochimica acta*, 2018, **185**, 201-201.
95. M. Li Liu, B. B. Chen, T. Yang, J. Wang, X. Dong Liu and C. Zhi Huang, *Methods and Applications in Fluorescence*, 2017, **5**, 015003.
96. H. He, Y. Ma, J. Li, X. Lai, X. Chen, L. Wang, W. Zhang, Y. Huang and P. Zhang, *journal of luminescence*, 2020, **221**.
97. G. Kaur, M. Chaudhary, K. C. Jena and N. Singh, *new journal of chemistry*, 2020, **44**, 10536-10544.
98. Q. Zhou, Y. Fang, J. Li, D. Hong, P. Zhu, S. Chen and K. Tan, *talanta*, 2021, **222**.
99. L. Li and T. Dong, *journal of materials chemistry c*, 2018, **6**, 7944-7970.
100. H. Chen, Y. Xie, A. M. Kirillov, L. Liu, M. Yu, W. Liu and Y. Tang, *chemical communications*, 2015, **51**, 5036-5039.
101. N. Amin, A. Afkhami and T. Madrakian, *journal of luminescence*, 2018, **194**, 768-777.
102. R. A. Tigaa, J. H. S. K. Monteiro, S. Silva-Hernandez and A. d. Bettencourt-Dias, *journal of luminescence*, 2017, **192**, 1273-1277.
103. H. Dong, A. Kuzmanoski, T. Wehner, K. Müller-Buschbaum and C. Feldmann, *materials*, 2016, **10**.
104. Y. Song, J. Chen, D. Hu, F. Liu, P. Li, H. Li, S. Chen, H. Tan and L. Wang, *sensors and actuators b chemical*, 2015, **221**, 586-592.
105. B. B. Chen, M. L. Liu, L. Zhan, C. M. Li and C. Z. Huang, *analytical chemistry*, 2018, **90**, 4003-4009.

106. M. L. Liu, B. B. Chen, J. H. He, C. M. Li, Y. F. Li and C. Z. Huang, *Talanta*, 2019, **191**, 443-448.
107. X. He, Y. Han, X. Luo, W. Yang, C. Li, W. Tang, T. Yue and Z. Li, *food chemistry*, 2020, **320**.
108. M. Xu, Z. Gao, Q. Zhou, Y. Lin, M. Lu and D. Tang, *Biosensors and Bioelectronics*, 2016, **86**, 978-984.
109. Z. Zhou, Q. Wang, J. Wang and C. C. Zhang, *carbon*, 2015, **93**, 671-680.
110. H. Yang, F. Lu, X. Zhan, M. Tian, Z. Yuan and C. Lu, *talanta*, 2020, **208**.
111. C. Zhang, H. Zhang, Y. Yu, S. Wu and F. Chen, *talanta*, 2019, **197**, 451-456.
112. J. Liu, X. Ge, L. Sun, R. Wei, J. Liu and L. Shi, *rsc advances*, 2016, **6**, 47427-47433.
113. Q. Chang, W. Xu, Q. Chen, C. Xue, N. Li, J. Yang and S. Hu, *applied surface science*, 2020, **508**, 144862.
114. J. Hao, F. Liu, N. Liu, M. Zeng, Y. Song and L. Wang, *sensors and actuators b chemical*, 2017, **245**, 641-647.
115. Y. Dong, J. Cai, Q. Fang, X. You and Y. Chi, *analytical chemistry*, 2016, **88**, 1748-1752.
116. Y. Wang, J. He, M. Zheng, M. Qin and W. Wei, *talanta*, 2019, **191**, 519-525.
117. X.-Y. Xu and B. Yan, *journal of materials chemistry c*, 2016, **4**, 1543-1549.
118. J.-X. Wu and B. Yan, *dalton transactions*, 2017, **46**, 7098-7105.
119. W. Li, H. Zhang, S. Chen, Y. Liu, J. Zhuang and B. Lei, *biosensors and bioelectronics*, 2016, **86**, 706-713.
120. X. Xu, W. Li, W. Zhou, G. Tan, Y. Zheng, C. Hu, B. Lei, X. Zhang, Y. Liu and J. Zhuang, *journal of materials chemistry c*, 2018, **6**, 10360-10366.
121. B. Lei, W. Li, H. Zhang, J. Wang, Y. Liu, J. Zhuang and S. Chen, *rsc advances*, 2015, **5**, 89238-89243.
122. X. Xu, X. Zhang, C. Hu, W. Li, B. Lei, Y. Liu and J. Zhuang, *journal of colloid and interface science*, 2019, **543**, 156-163.
123. Y. He, J. He, H. Zhang, Y. Liu and B. Lei, *journal of colloid and interface science*, 2017, **496**, 8-15.
124. A. Zhou, F. Song, W. Yao, Y. Han, F. Song, W. Wu, C. Ming, D. Ju and A. Khan, *journal of alloys and compounds*, 2019, **775**, 457-465.
125. M. Li, W. Yao, J. Liu, Q. Tian, L. Liu, J. Ding, Q. Xue, Q. Lu and W. Wu, *journal of materials chemistry c*, 2017, **5**, 6512-6520.
126. B. Chen and J. Feng, *journal of physical chemistry c*, 2015, **119**, 7865-7872.
127. Y. Wang, K. Čépe and R. Zbořil, *journal of materials chemistry c*, 2016, **4**, 7253-7259.
128. J. He, Y. He, J. Zhuang, H. Zhang, B. Lei and Y. Liu, *optical materials*, 2016, **62**, 458-464.
129. Y. Xu, X.-H. Jia, X.-B. Yin, X.-W. He and Y.-K. Zhang, *analytical chemistry*, 2014, **86**, 12122-12129.
130. N. Gong, H. Wang, S. Li, Y. Deng, X. a. Chen, L. Ye and W. Gu, *langmuir*, 2014, **30**, 10933-10939.
131. H. Liao, Z. Wang, S. Chen, H. Wu, X. Ma and M. Tan, *rsc advances*, 2015, **5**, 66575-66581.
132. Y. Huang, L. Li, D. Zhang, L. Gan, P. Zhao, Y. Zhang, Q. Zhang, M. Hua and C. Jia, *magnetic resonance imaging*, 2020, **68**, 113-120.
133. H. Chen, L. Wang, H. Fu, Z. Wang, Y. Xie, Z. Zhang and Y. Tang, *journal of materials chemistry b*, 2016, **4**, 7472-7480.
134. C. Yu, T. Xuan, Y. Chen, Z. Zhao, X. Liu, G. Lian and H. Li, *journal of alloys and compounds*, 2016, **688**, 611-619.
135. A. B. Bourlinos, A. Bakandritsos, A. Kouloumpis, D. Gournis, M. Krysmann, E. P. Giannelis, K. Polakova, K. Safarova, K. Hola and R. Zboril, *journal of materials chemistry*, 2012, **22**, 23327-23330.
136. Y. Pan, J. Yang, Y. Fang, J. Zheng, R. Song and C. Yi, *journal of materials chemistry b*, 2017, **5**, 92-101.
137. D. Bouzas-Ramos, J. C. Canga, J. C. Mayo, R. M. Sainz, J. R. Encinar and J. M. Costa-Fernandez, *advanced functional materials*, 2019, **29**.
138. H. Chen, G. D. Wang, W. Tang, T. Todd, Z. Zhen, C. Tsang, K. Hekmatyar, T. Cowger, R. B. Hubbard, W. Zhang, J. Stickney, B. Shen and J. Xie, *advanced materials*, 2014, **26**, 6761-6766.
139. F. Du, L. Zhang, L. Zhang, M. Zhang, A. Gong, Y. Tan, J. Miao, Y. Gong, M. Sun, H. Ju, C. Wu and S. Zou, *biomaterials*, 2017, **121**, 109-120.
140. H. Chen, G. D. Wang, X. Sun, T. Todd, F. Zhang, J. Xie and B. Shen, *advanced functional materials*, 2016, **26**, 3973-3982.
141. Y. Wu, H. Li, Y. Yan, K. Wang, Y. Cheng, Y. Li, X. Zhu, J. Xie and X. Sun, *international journal of nanomedicine*, 2020, **15**, 4691-4703.
142. D. Li, P. Jing, L. Sun, Y. An, X. Shan, X. Lu, D. Zhou, D. Han, D. Shen, Y. Zhai, S. Qu, R. Zbořil and A. L. Rogach, *advanced materials*, 2018, **30**.
143. Z. Wang, F. Yuan, X. Li, Y. Li, H. Zhong, L. Fan and S. Yang, *advanced materials*, 2017, **29**.
144. H. Xu, X. Rao, J. Gao, J. Yu, Z. Wang, Z. Dou, Y. Cui, Y. Yang, B. Chen and G. Qian, *chemical communications*, 2012, **48**, 7377-7379.
145. C. Tan, Q. Wang and C. C. Zhang, *chemical communications*, 2011, **47**, 12521-12523.
146. B. Ma, F. Zeng, F. Zheng and S. Wu, *analyst*, 2011, **136**, 3649-3655.
147. J. Wang, D. Li, Y. Qiu, X. Liu, L. Huang, H. Wen and J. Hu, *talanta*, 2020, **220**.
148. L. Zhang, Z. Wang, J. Zhang, C. Shi, X. Sun, D. Zhao and B. Liu, *nanomaterials*, 2019, **9**.
149. S.-J. Qin and B. Yan, *sensors and actuators b chemical*, 2018, **272**, 510-517.
150. W. Lu, X. Qin, S. Liu, G. Chang, Y. Zhang, Y. Luo, A. M. Asiri, A. O. Al-Youbi and X. Sun, *analytical chemistry*, 2012, **84**, 5351-5357.
151. H. M. R. Gonçalves, A. J. Duarte and J. C. G. E. d. Silva, *biosensors and bioelectronics*, 2010, **26**, 1302-1306.
152. S. Barman and M. Sadhukhan, *journal of materials chemistry*, 2012, **22**, 21832-21837.
153. M. Zhang, W. Wang, P. Yuan, C. Chi, J. Zhang and N. Zhou, *chemical engineering journal*, 2017, **330**, 1137-1147.
154. H. Wu and C. Tong, *analytical chemistry*, 2020, **92**, 8859-8866.
155. Y. Y. Liang, *analytical chemistry*, 1990, **62**, 2504-2506.
156. D. Mao, X. Liu, Q. Qiao, W. Yin, M. Zhao, J. M. Cole, J. Cui and Z. Xu, *analyst*, 2015, **140**, 1008-1013.
157. X. Lian, D. Zhao, Y. Cui, Y. Yang and G. Qian, *chemical communications*, 2015, **51**, 17676-17679.
158. D. Zhou, D. Liu, W. Xu, X. Chen, Z. Yin, X. Bai, B. Dong, L. Xu and H. Song, *chemistry of materials*, 2017, **29**, 6799-6809.
159. C. Chen, Y. Yu, C. Li, D. Liu, H. Huang, C. Liang, Y. Lou, Y. Han, Z. Shi and S. Feng, *small*, 2017, **13**.
160. J. Zhang, F. Song, Z. He, Y. Liu, Z. Chen, S. Lin, L. Huang and W. Huang, *small*, 2016, **12**, 397-404.
161. Z. Song, T. Lin, L. Lin, S. Lin, F. Fu, X. Wang and L. Guo, *angewandte chemie*, 2016, **55**, 2773-2777.

162. K. Jiang, L. Zhang, J. Lu, C. Xu, C. Cai and H. Lin, *angewandte chemie*, 2016, **55**, 7231-7235.
163. P. Kumar, S. Singh and B. K. Gupta, *nanoscale*, 2016, **8**, 14297-14340.
164. R. S. Li, J. H. Liu, T. Yang, P. F. Gao, J. Wang, H. Liu, S. J. Zhen, Y. F. Li and C. Z. Huang, *analytical chemistry*, 2019, **91**, 11185-11191.
165. B. Chen, H. Xie, S. Wang, Z. Guo, Y. Hu and H. Xie, *luminescence*, 2019, **34**, 437-443.
166. Y.-P. Sun, B. Zhou, Y. Lin, W. Wang, K. A. S. Fernando, P. Pathak, M. J. Meziani, B. A. Harruff, X. Wang, H. Wang, P. G. Luo, H. Yang, M. E. Kose, B. Chen, L. M. Veca and S.-Y. Xie, *journal of the american chemical society*, 2006, **128**, 7756-7757.
167. P. G. Luo, S. Sahu, S.-T. Yang, S. K. Sonkar, J. Wang, H. Wang, G. E. LeCroy, L. Cao and Y.-P. Sun, *Journal of Materials Chemistry B*, 2013, **1**, 2116-2127.
168. K. Jiang, S. Sun, L. Zhang, Y. Lu, A. Wu, C. Cai and H. Lin, *angewandte chemie*, 2015, **54**, 5360-5363.
169. C. Kalavagunta, S. Michaeli and G. J. Metzger, *contrast media & molecular imaging*, 2014, **9**, 169-176.
170. H. S. Choi, W. Liu, F. Liu, K. Nasr, P. Misra, M. G. Bawendi and J. V. Frangioni, *nature nanotechnology*, 2010, **5**, 42-47.
171. J. Gao, K. Chen, R. Luong, D. M. Bouley, H. Mao, T. Qiao, S. S. Gambhir and Z. Cheng, *nano letters*, 2012, **12**, 281-286.
172. Y. Ye and X. Chen, *theranostics*, 2011, **1**, 102-126.
173. X. Ren, L. Liu, Y. Li, Q. Dai, M. Zhang and X. Jing, *journal of materials chemistry b*, 2014, **2**, 5541-5549.
174. L. Zhou, X. Zheng, Z. Gu, W. Yin, X. Zhang, L. Ruan, Y. Yang, Z. Hu and Y. Zhao, *biomaterials*, 2014, **35**, 7666-7678.
175. Z. Liu, Z. Li, J. Liu, S. Gu, Q. Yuan, J. Ren and X. Qu, *biomaterials*, 2012, **33**, 6748-6757.
176. T. Lammers, F. Kiessling, W. E. Hennink and G. Storm, *molecular pharmaceutics*, 2010, **7**, 1899-1912.
177. D. A. Jaffray, *nature reviews clinical oncology*, 2012, **9**, 688-699.
178. S. Dufort, A. Bianchi, M. Henry, F. Lux, G. L. Duc, V. Josserand, C. Louis, P. Perriat, Y. Crémillieux, O. Tillement and J.-L. Coll, *small*, 2015, **11**, 215-221.
179. M. A. Dobrovolskaia, D. R. Germolec and J. L. Weaver, *Nat Nanotechnol*, 2009, **4**, 411-414.
180. M. A. Dobrovolskaia and S. E. McNeil, *Nat Nanotechnol*, 2007, **2**, 469-478.
181. K. C. Nguyen, V. L. Seligy and A. F. Tayabali, *Nanotoxicology*, 2013, **7**, 202-211.
182. Z. Liu, C. Davis, W. Cai, L. He, X. Chen and H. Dai, *Proc Natl Acad Sci U S A*, 2008, **105**, 1410-1415.
183. K. Yang, H. Gong, X. Shi, J. Wan, Y. Zhang and Z. Liu, *Biomaterials*, 2013, **34**, 2787-2795.
184. B. C. Nelson, M. E. Johnson, M. L. Walker, K. R. Riley and C. M. Sims, *antioxidants*, 2016, **5**.
185. M. Zhang, C. Zhang, X. Zhai, F. Luo, Y. Du and C. Yan, *science china materials*, 2019, **62**, 1727-1739.
186. M. Zhang, L. Zhao, F. Du, Y. Wu, R. Cai, L. Xu, H. Jin, S. Zou, A. Gong and F. Du, *nanotechnology*, 2019, **30**.
187. P.-C. Hsu, Z.-Y. Shih, C.-H. Lee and H.-T. Chang, *green chemistry*, 2012, **14**, 917-920.
188. A. M. Vostrikova, A. A. Kokorina, P. A. Demina, S. V. German, M. V. Novoselova, N. V. Tarakina, G. B. Sukhorukov and I. Y. Goryacheva, *scientific reports*, 2018, **8**, 1-8.
189. Y. Dong, H. Pang, H. B. Yang, C. Guo, J. Shao, Y. Chi, C. M. Li and T. Yu, *angewandte chemie*, 2013, **52**, 7800-7804.
190. L. He, T. Wang, J. An, X. Li, L. Zhang, L. Li, G. Li, X. Wu, Z. Su and C. Wang, *crystengcomm*, 2014, **16**, 3259-3263.
191. B. Dai, D. Deng, H. Yu, L. Lei, Y. Li, C. Li and S. Xu, *rsc advances*, 2016, **6**, 72149-72154.
192. K. Yi, X. Zhang and L. Zhang, *science of the total environment*, 2020, **743**.
193. Y. Fang, S. Guo, D. Li, C. Zhu, W. Ren, S. Dong and E. Wang, *acs nano*, 2012, **6**, 400-409.
194. Q. Wen, Z. Zeng, W. Liu, J. Gao, H. M. Zhang, C. C. Zhang and Y. Zheng, *synthetic metals*, 2019, **257**.
195. A. B. Bourlinos, A. Stassinopoulos, D. Anglos, R. Zboril, V. Georgakilas and E. P. Giannelis, *chemistry of materials*, 2008, **20**, 4539-4541.
196. A. H. Loo, Z. Sofer, D. Bouša, P. Ulbrich, A. Bonanni and M. Pumera, *acs applied materials & interfaces*, 2016, **8**, 1951-1957.
197. Y. Fang, L. Zhou, J. Zhao, Y. Zhang, M. Yang and C. Yi, *Carbon*, 2020, **166**, 265-272.
198. S. Zheng, N. Yu, C. Han, T. Xie, B. Dou, Y. Kong, F. Zuo, M. Shi and K. Xu, *Biochemical and Biophysical Research Communications*, 2019, **511**, 207-213.
199. Y. Wu, Y. Yan, X. Gao, L. Yang, Y. Li, X. Guo, J. Xie, K. Wang and X. Sun, *Nanomedicine: Nanotechnology, Biology and Medicine*, 2019, **21**, 102074.
200. Y. Fang, J. Jia, J. Yang, J. Zheng and C. Yi, *Chinese Chemical Letters*, 2018, **29**, 1277-1280.
201. Y. Fang, L. Zhou, J. Yang, J. Zhao, Y. Zhang and C. Yi, *Journal*, 2020, **3**, 3761-3769.

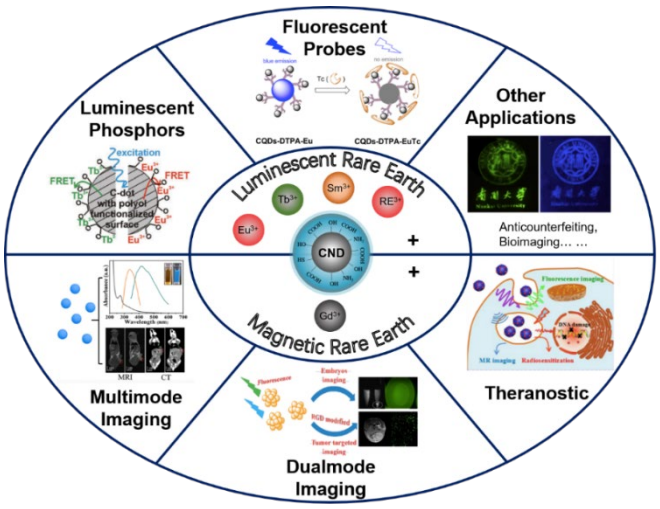

Fig. 1 Schematic illustration of different application areas of RE-CNDs

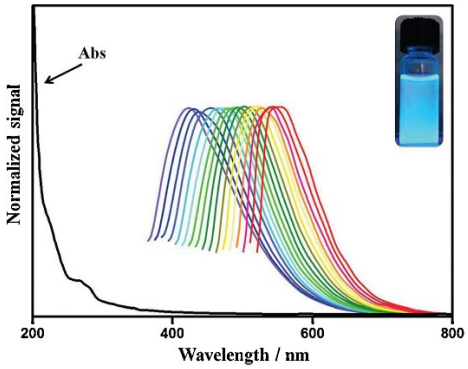

Fig. 2 Absorption and excitation-dependent PL spectra of CNDs, with gradually increased excitation wavelengths (in 15 nm increments beginning from 350 nm). Inset: photographs of the CNDs solution under a UV lamp (365 nm). The PL intensities are normalized in arbitrary units. (Reproduced with permission from ref. [187]. Copyright 2012 Royal Society of Chemistry.)

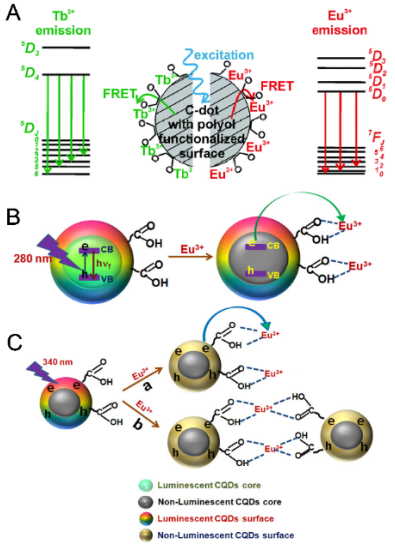

Fig. 3 (A) Schematic illustration of the FRET process between CNDs and RE^{3+}. (Reproduced with permission from ref. [55]. Copyright 2014 Royal Society of Chemistry.) (B) Photo-induced excitation of core states of CNDs and the electron transfer to Eu^{3+}. (C) Photo-induced excitation of surface states of CNDs and the electron transfer to Eu^{3+} (a) and the aggregation of CNDs upon addition of Eu^{3+} (b). (Reproduced with permission from ref. [54]. Copyright 2017 American Chemical Society.)

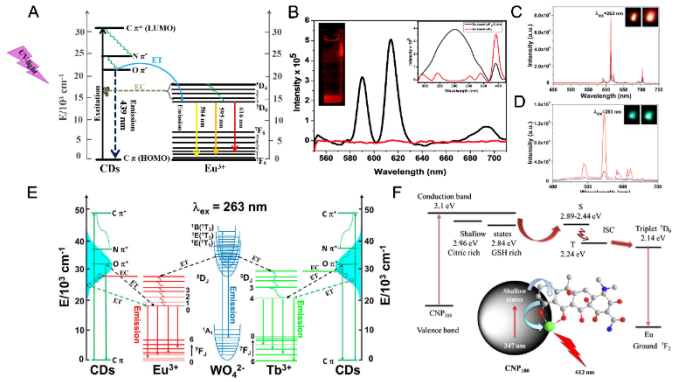

Fig. 4 (A) Schematic illustration of the energy transfer mechanism of CNDs/YF_3: RE^{3+} (RE = Eu or Tb). (Reproduced with permission from ref. [60]. Copyright 2020 Elsevier Ltd.) (B) The PL spectra of CNDs/LaF_3:Eu^{3+} (black line) and LaF_3:Eu^{3+} (red line). Left inset: photographs of the nanocomposites under UV excitation. Right inset: the excitation spectra of the nanocomposites under UV excitation. (Reproduced with permission from ref. [61]. Copyright 2015 Royal Society of Chemistry.) (C) Emission spectra of CNDs@$MgWO_4$:12%Eu^{3+} (red line) and $MgWO_4$:12%Eu^{3+} (black line). Inset: photographs of $MgWO_4$:Eu^{3+} (left) and CNDs@$MgWO_4$:Eu^{3+} (right) under the excitation of 263 nm. (D) Emission spectra of CNDs@$MgWO_4$:8%Tb^{3+} (red line) and $MgWO_4$:8%Tb^{3+} (black line). Inset: photographs of $MgWO_4$:Tb^{3+} (left) and CNDs@$MgWO_4$:Tb^{3+} (right) under the excitation of 263 nm. (E) Schematic illustration of the energy transfer process from WO_4^{2-}, CNDs to RE^{3+}, the electron capture process of CNDs and the emission process from CNDs, Eu^{3+} and Tb^{3+}. (Reproduced with permission from ref. [64]. Copyright 2018 American Chemical Society.) (F) Schematic illustration of the energy transfer process between CNDs and EuTC complex. (Reproduced with permission from ref. [53]. Copyright 2015 Elsevier Ltd.)

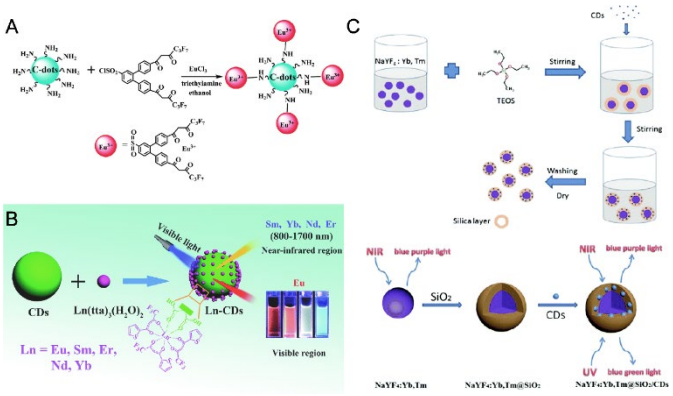

Fig. 5 (A) Synthesis of CNDs-BHHCT-Eu^{3+} (Reproduced with permission from ref. [89]. Copyright 2014 Royal Society of Chemistry.) (B) Schematic illustration of the synthesis and emission of RE-CNDs (RE = Eu^{3+}, Sm^{3+}, Er^{3+}, Yb^{3+}, Nd^{3+}) from visible to NIR region. (Reproduced with permission from ref. [112]. Copyright 2016 Royal Society of Chemistry.) (C) Schematic illustration for the preparation of $NaYF_4$:Yb,Tm@CNDs composites. (Reproduced with permission from ref. [120]. Copyright 2018 Royal Society of Chemistry.)

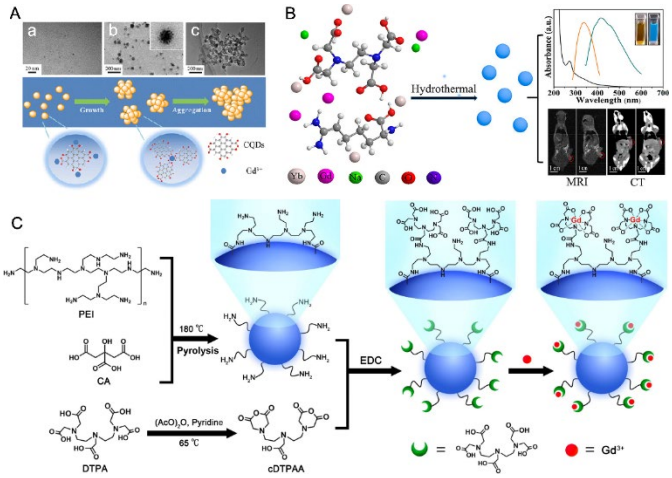

Fig. 6 (A) TEM images of Gd-CNDs after different times of hydrothermal treatment: (a) 1h, (b) 3h, and (c) 5h, and the schematic illustration for the formation process of Gd-CNDs. (Reproduced with permission from ref. [129]. Copyright 2014 American Chemical Society.) (B) Schematic illustration for the fabrication and applications of Gd/Yb-CNDs for fluorescence, MRI and CT imaging. (Reproduced with permission from ref. [87]. Copyright 2018 American Chemical Society.) (C) Schematic illustration for the fabrication process of Gd-DTPA-CNDs. (Reproduced with permission from ref. [86]. Copyright 2015 Elsevier Ltd.)

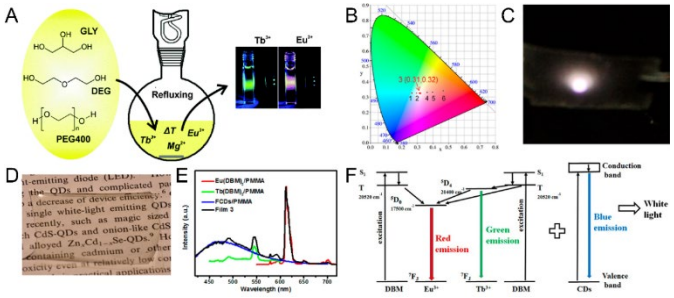

Fig. 7 (A) Illustration of the synthesis procedure of Tb/Eu-CNDs. On the right are the photographs of Tb-CNDs and Eu-CNDs under blue LED excitation (λ_{max} = 465 nm). (Reproduced with permission from ref. [55]. Copyright 2014 Royal Society of Chemistry.) (B) CIE chromatic diagram of the prepared film. (C) Photographs of white light emitting film under 400 nm excitation. (D) Photograph of white light emitting film under sunlight. (E) PL spectra of PMMA film with different compositions. (F) The energy transfer mechanism of white light emitting film. (Reproduced with permission from ref. [126]. Copyright 2015 American Chemical Society.)

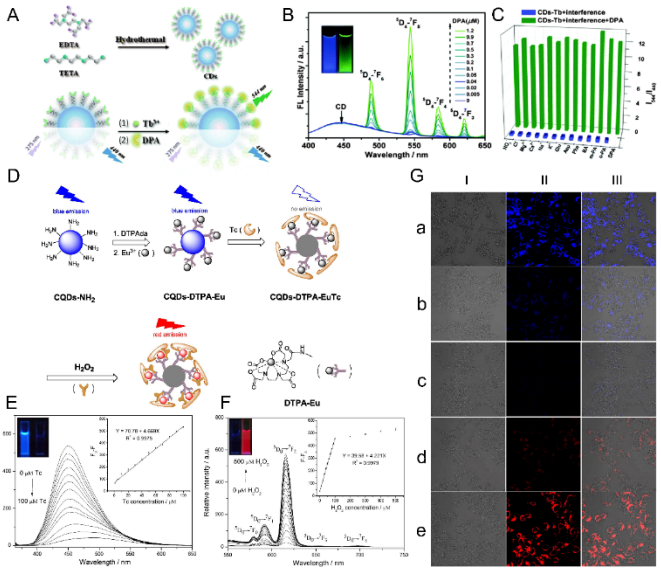

Fig. 8 (A) Synthesis route of CNDs with functional groups and mechanism of Tb-CNDs for the detection of DPA. (B) PL spectra of Tb-CNDs upon the increasing of DPA measured under 275 nm excitation. Inset: photographs of Tb-CNDs taken under the excitation of 245 nm UV lamp before (left) and after (right) the addition of 50 μM DPA. (C) The fluorescence of Tb-CNDs in response to the interference of aromatic carboxylic acids, amino acids and bio-relevant ions. The blue bars show the addition of 10 μM interfering molecules or ions into Tb-CNDs solution (30 μg/mL, pH = 7.0 HCl-Tris buffer solution). The green bars show the fluorescence after adding 10 μM of DPA into the solution (λ_{ex} = 275 nm). (Reproduced with permission from ref. 101. Copyright 2015 Royal Society of Chemistry.) (D) Schematic illustration for the mechanism of the fluorescent probe CNDs-DTPA-Eu with the luminescent quenching by TC and subsequent enhancement by H_2O_2. (E) PL spectra of CNDs-DTPA-Eu upon addition of TC in PBS buffer solution (pH 7.4). Left inset: CNDs-DTPA-Eu solution without (left) and with (right) 100 μM TC (λ_{ex} = 365 nm). Right inset: plots of fluorescent intensity (F_0-F) versus TC concentration. (F) PL spectra of CNDs-DTPA-Eu-TC upon addition of H_2O_2 in PBS buffer solution (pH 7.4). Left inset: CNDs-DTPA-Eu-TC solution without (left) and with (right) 500 μM H_2O_2 (λ_{ex} = 405 nm). Right inset: plots of fluorescent intensity (F_0-F) versus H_2O_2 concentration. (G) Confocal fluorescence images of Hela cells incubated with CNDs-DTPA-Eu before (a) and after the addition of TC (b: 50 μM; c: 100 μM) and H_2O_2 (d: 50 μM; e: 100 μM). (I) bright field; (II) blue channel; (III) overlap. (Reproduced with permission from ref. [109]. Copyright 2015 Elsevier Ltd.)

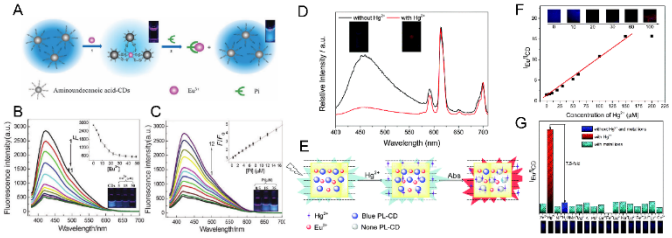

Fig. 9 (A) Schematic illustration of the Pi detection based on the off-on fluorescent probe of Eu-CNDs. (B) PL spectra of CNDs quenched by different amounts of Eu^{3+}. Inset: PL intensity at 420 nm with the titration of Eu^{3+}. Inset photographs: Colour change of the solutions under UV-lamp. (C) PL spectra of Eu-CNDs recovered with different amounts of Pi. Inset: PL intensity at 420 nm with the titration of Pi. Inset photographs: Colour change of the solutions under UV-lamp. (Reproduced with permission from ref. [51]. Copyright 2011 Royal Society of Chemistry.) (D) PL spectra of CNDs/Eu@MOFs before (black) and after (red) the addition of Hg^{2+} (λ_{ex} = 360 nm). Inset: photographs under 365 nm UV light. (E) Schematic illustration of the mechanism for Hg^{2+} detection by CNDs/Eu@MOFs. (F) Linear correlation of PL intensity (I_{Eu}/I_{CNDs}) with different amounts of Hg^{2+}. Inset: photographs of the colour change. (G) PL spectra of I_{Eu}/I_{CNDs} for CNDs/Eu@MOFs solutions with different metal ions (100 μM, λ_{ex} = 360 nm). Inset: photographs under 365 nm UV light. (Reproduced with permission from ref. [117]. Copyright 2016 Royal Society of Chemistry.)

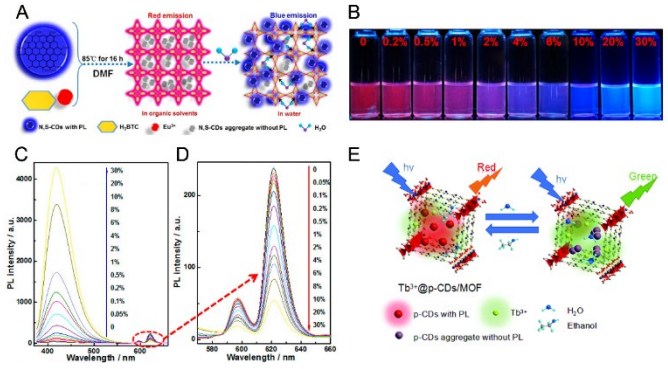

Fig. 10 (A) Synthesis routes of CNDs/Eu-MOFs and detection of water in organic solvents. (B) Photographs of the visualized change in PL of 1 mg/mL CNDs/Eu-MOFs in ethanol with different water content (V/V) under 365 nm excitation. (C) PL spectra of the 1 mg/mL CNDs/Eu-MOFs in ethanol upon the addition of water. (D) Amplification of the Eu^{3+} emission peaks in (C). (Reproduced with permission from ref. [115]. Copyright 2016 American Chemical Society.) (E) Schematic illustration of the mechanism of PL response for water sensing in organic solvent of CNDs/Tb@MOFs. (Reproduced with permission from ref. [118]. Copyright 2017 Royal Society of Chemistry.)

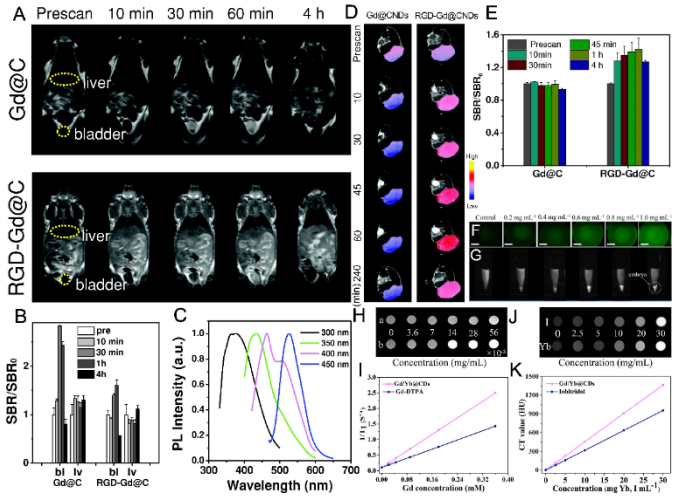

Fig. 11 (A) T_1-weighted MR images of normal nude mice taken at different time nodes after the injection of Gd-CNDs and RGD-Gd-CNDs. (B) Region of interest (ROI) analysis of the signal change in the bladder (bl) and liver (lv) based on images from (A). (C) PL of urine samples taken 60 min after the injection of RGD-Gd-CNDs. (D) T_1-weighted coronal MR images after the injection of RGD-Gd-CNDs and Gd-CNDs. (E) The relative signal variation at different time nodes based on the images from (D). (Reproduced with permission from ref. [138]. Copyright 2014 Wiley VCH.) (F) Fluorescence and (G) MR images of zebrafish embryos treated by Gd-CNDs with different concentrations. Scale bar: 250 μm. (Reproduced with permission from ref. [129]. Copyright 2014 American Chemical Society.) (H) MR phantom images and (I) changes of relaxation rate of Gd-DTPA (a) and Gd/Yb-CNDs (b) with different concentrations of Gd^{3+}. (J) CT phantom images and (K) Hounseld unit (HU) values of Gd/Yb-CNDs and iobitridol solution with different concentrations of Yb^{3+} and I, respectively. (Reproduced with permission from ref. [87]. Copyright 2018 American Chemical Society.)

Table 1 Overview of the one-step synthesis methods to obtain RE-CNDs

RE-CNDs	Precursors of CNDs	Surface groups on CNDs	RE^{3+}	Synthesis method	A
RE-CNDs	PEG400 Diethylene glycol Glycerol	-OH	Eu^{3+} or Tb^{3+}	Heating	
CNDs/LaF_3:Eu^{3+}	Triethylene glycol	-	Eu^{3+}	Hydrothermal	
RE-CNDs	Citric acid Ethanediamine	-OH, -COOH, $-NH_2$,	Yb^{3+} or Nd^{3+}	Hydrothermal	
Eu/Tb-CNDs	EDTA-4Na	-OH, -COOH, $-NH_2$,	Eu^{3+} and/or Tb^{3+}	Hydrothermal	
Eu-CNDs	PEG400	-COOH	Eu^{3+}	Microwave-assisted polyol synthesis	
RE-CNDs	Europium citrate chelate	-OH, -COOH	Eu^{3+} and/or Tb^{3+}	Hydrothermal	
Tb-CNDs	Sodium dextran sulfate	-COOH, $-SO_3$	Tb^{3+}	Three different methods	
CNDs/HAp:Eu,Gd	Sodium citrate Ethanediamine	-OH, -COOH, $-NH_2$,	Eu^{3+}, Gd^{3+}	Hydrothermal	
Eu-CNDs	Citric acid	-OH, -COOH	Eu^{3+}	Pyrolysis	
Eu-CNDs	Glutathione Formamide	-OH, -COOH	Eu^{3+}	Solvothermal	
Eu-CNDs	Citric acid	-OH, -COOH	Eu^{3+}	Carbonization	
Tb-CNDs	Citric acid	-OH, -COOH	Tb^{3+}	Hydrothermal	
La-CNDs	ATP	-OH, -COOH, $-NH_2$, $-PO_4^{3-}$	La^{3+}	Hydrothermal	
Eu-CNDs	EDTA L-cysteine	-OH, -COOH, $-NH_2$, $-SH^-$	Eu^{3+}	Microwave-assisted hydrothermal	

Table 2 Overview of the multi-step synthesis methods to obtain RE-CNDs.

RE-CNDs	Precursors of CNDs	Surface groups on CNDs	Synthesis of CNDs	RE^{3+}
EuTC-CNDs	Citric acid Glutathione	-OH, -COOH, $-NH_2$, -SH	Hydrothermal	Eu^{3+}
CNDs/$MgWO_4$:Eu	Citric acid Urea	-OH, -COOH, $-NH_2$	Hydrothermal	Eu^{3+}
CNDs/$MgWO_4$:RE	Citric acid Urea	-OH, -COOH, $-NH_2$	Hydrothermal	Eu^{3+} or Tb^{3+}
CNDs/$ZnGa_2O_4$:Eu	Citric acid Urea	-OH, -COOH, $-NH_2$	Microwave	Eu^{3+}
CNDs/$Eu(DPA)_3$/$Tb(DPA)_3$-PVA	Citric acid L-cysteine	-OH, -COOH, $-NH_2$, -SH	[189]	$Eu(DPA)_3$ and $Tb(DPA)_3$
CNDs/Eu^{3+}/PVA	EDTA-2Na	-OH, -COOH, $-NH_2$	One-step pyrolytic route	Eu^{3+}
CNDs/$Eu(DBM)_3$/$Tb(DBM)_3$-PMMA	Acrylic acid Ethanediamine	-OH, -COOH, $-NH_2$	Microwave-assisted pyrolysis	$Eu(DBM)_3$ and $Tb(DBM)_3$
CNDs/YF_3: RE^{3+}	Citric acid Urea	-OH, -COOH, $-NH_2$	Hydrothermal	Eu^{3+} and/or Tb^{3+}
$NaYF_4$:Eu@CNDs	Anhydrous citric acid AEAPMS	-CONH-, Methoxysilane groups	Hydrothermal	Eu^{3+}
$NaYF_4$:Yb,Er(Tm)@SiO_2/CNDs	Citric acid Thiourea	-OH, -COOH, -SCN	Hydrothermal	Yb^{3+}, Er^{3+}, Tm^{3+}
$NaYF_4$:Yb,Tm@SiO_2/CNDs	Anhydrous citric acid AEAPMS	$-NH_2$, Methoxysilane group	Hydrothermal	Yb^{3+}, Tm^{3+}
CNDs/$NaLuF_4$:Yb,Er	Citric acid Ethanediamine	-OH, -COOH, $-NH_2$, -CONH-	Hydrothermal	Yb^{3+}, Er^{3+}
RE-CNDs-	Acetic acid P_2O_5	-COOH	190	Eu^{3+} or Tb^{3+}
~~Eu~~-CNDs-EDTA-Eu	Citric acid Ethylenediamine	-OH, -COOH, $-NH_2$	Hydrothermal	Eu^{3+}
CNDs/Eu/ionogel	Acetamide Anhydrous ethanol	-OH, -COOH, $-NH_2$, -CONH	Pyrolysis	Eu^{3+}

RE-CNDs	Precursors of CNDs	Surface groups on CNDs	Synthesis of CNDs	RE^{3+}
Tb-CNDs	Citric acid TETA	-OH, -COOH, $-NH_2$, -CONH-	Hydrothermal	Tb^{3+}
Tb-CNDs	EDTA TETA	-COOH, $-NH_2$	Hydrothermal	Tb^{3+}
Tb-CNDs	Citric acid TETA	-OH, -COOH, $-NH_2$, -CONH-	Hydrothermal	Tb^{3+}
Tb-CNDs	Schizochytrium	-COOH, $-NH_2$	Hydrothermal	Tb^{3+}
CNDs-Eu/GMP	Chitosan Acetic acid	-OH, -COOH, $-NH_2$	Hydrothermal	Eu^{3+}
CNDs-EDTA-Eu	Citric acid hPEI (1800Da)	-OH, -COOH, $-NH_2$	Hydrothermal	Eu^{3+}
Eu-CNDs	Citric acid monohydrate Urea	-COOH, $-NH_2$	Microwave-assisted hydrothermal	Eu^{3+}
CNDs@Eu-MOFs	Citric acid Urea	-COOH, $-NH_2$	Hydrothermal	Eu^{3+}
CNDs/Eu@MOFs(MIL-53-COOH)	Citric acid Ethanediamine	-OH, -COOH, $-NH_2$	Hydrothermal	Eu^{3+}
CNDs/YVO_4:Eu@MIP	Anhydrous citric acid AEAPMS	-COOH, $-NH_2$	Hydrothermal	Eu^{3+}
CNDs-DTPA-Eu	Citric acid Ethanediamine	-OH, -COOH, $-NH_2$	Microwave	Eu^{3+}
CNDs-calcein-Eu	Ethanolamine	-OH, -COOH, $-NH_2$, -CONH	Pyrolysis	Eu^{3+}
Tb-CNDs	Glucose PEG-200	-COOH	Microwave	Tb^{3+}
Eu-CNDs	3-hydroxybenzoic acid	-COOH	Hydrothermal	Eu^{3+}
Eu-CNDs	$H_2N(CH_2)_{10}COOH$ Citric acid	-COOH	Thermal oxidation [195]	Eu^{3+}
CNDs/Eu@MOFs-253	Citric acid Ethanediamine	-OH, -COOH, $-NH_2$	Hydrothermal	Eu^{3+}
CNDs-Tb-DPA	Citric acid Urea	-OH, -COOH, $-NH_2$, -CONH	Hydrothermal	Tb-DPA
CNDs-Tb/APBA	Nicotinic acid barbituric acid	-OH, -COOH, $-NH_2$	Hydrothermal	Tb^{3+}
CNDs/Eu-DPA MOFs	Chitosan	-OH, $-NH_2$	Hydrothermal	Eu^{3+}
CNDs-BHHCT-Eu	Chitosan	-OH, $-NH_2$	Hydrothermal	Eu^{3+}
Eu-CNDs	Citric acid	-OH, -COOH	[196]	Eu^{3+}

Surface groups on CNDs	Synthesis of CNDs	RE^{3+}	Synthesis method	Coating	Applications
$-NH_2$	Microwave	Eu^{3+}	-	-	Cr^{6+} detection
-OH, -COOH, $-NH_2$	Hydrothermal	Eu^{3+}	Mixing	-	SeO_3^{2-} detection
-OH, -COOH, $-NH_2$, -SH	Hydrothermal	Eu^{3+}	-	-	Water detection
-	Solvothermal	Tb^{3+}	*In situ* post-synthetic modification procedure	-	Water and moisture detection
$-Si-OCH_3$	Hydrothermal	Eu^{3+}, Dy^{3+}	Sol-gel methods	-	Temperature sensing
$-NH_2$, -OH	Hydrothermal	Eu^{3+}	Mixing	-	Temperature sensing
-COOH, $-NH_2$	Pyrolysis	Eu^{3+}	Mixing	PVA	Anti-counterfeiting
-COOH	Hydrothermal	Eu^{3+}	Mixing	PVA	Anti-counterfeiting
-OH, -COOH, $-NH_2$	Sovothermel	Er^{3+}, Yb^{3+}(Tm^{3+})	Solvothermal	PAA	Anti-counterfeiting

Table 3 Overview of the synthesis and applications of Gd-CNDs.

Hybrids	Precursors	Synthesis of RE-CNDs	RE^{3+}	Relaxivity (r_1)/mM^{-1} s^{-1}	Field (T)	Applications	Notes	Ref.
Gd-CNDs	Tris base Betaine hydrochloride Gadopentetic acid	Pyrolysis	Gd^{3+}	-	-	MRI/Fluorescence dual-mode imaging probe	Tris-base = tris(hydroxymethyl)amino methane	135
Gd-CNDs	Gd-DTPA	Calcination	Gd^{3+}	5.88	7.0	MRI/Fluorescence dual-mode imaging probe		138
Gd-CNDs	Citric acid Ethanediamine $GdCl_3$	One-pot hydrothermal	Gd^{3+}	7.36	1.2	MRI/Fluorescence dual-mode imaging probe		129
Gd-CNDs	GdPM	One-step pyrolysis	Gd^{3+}	6.4	3.0	MRI/Fluorescence dual-mode imaging probe	GdPM = gadopentetate monomeglumine	
Gd-CNDs	Sucrose DEG $GdCl_3$	One-step microwave-assisted polyol method	Gd^{3+}	11.356	7.0	MRI/Fluorescence dual-mode imaging probe	DEG = Diethylene glycol	130
Gd-DTPA-CNDs	Citric acid PEI cDTPAda $GdCl_3$	Coordination	Gd^{3+}	56.72	3.0	MRI/Fluorescence dual-mode imaging probe	PEI = polyethyl-enimine cDTPAda = cyclic DTPA dianhydride	86
Gd-CNDs	Citric acid $GdCl_3$	One-pot hydrothermal	Gd^{3+}	14.08	-	MRI/Fluorescence dual-mode imaging probe		131
Gd-CNDs	Citric acid Ethanediamine $GdCl_3$	One-pot hydrothermal	Gd^{3+}	6.06	0.5	MRI/Fluorescence dual-mode imaging probe		133
Gd-CNDs	Citric acid DETA $GdCl_3$	One-pot hydrothermal	Gd^{3+}	14.33	0.5	MRI/Fluorescence dual-mode imaging probe	DETA = diethylenetriamine	134
Gd-CNDs	$Gd(NO_3)_3$ Gd-DTPA	MSN-templated method	Gd^{3+}	10	7	MRI/Fluorescence dual-mode imaging probe		140
Gd-CNDs	Citric acid BPEI Gd-DTPA	One-pot pyrolysis	Gd^{3+}	57.42	1.5	MRI/Fluorescence dual-mode imaging probe	BPEI = branched-polyethylenimine	136
Gd-CNDs	Citric acid Urea $GdCl_3$	Solvothermal	Gd^{3+}	16.428	1.5	MRI/Fluorescence dual-mode imaging probe		197
Gd-CNDs	Gd-DTPA L-arginine	One-pot solvent free method	Gd^{3+}	6.27	3.0	MRI/Fluorescence dual-mode imaging probe		198

Hybrids	Precursors	Synthesis of RE-CNDs	RE^{3+}	Relaxivity (r_1)/mM^{-1} s^{-1}	Field (T)	Applications	Notes	Ref.
Gd-CNDs	-	-	Gd^{3+}	10.0	3.0	DCE-MRI to non-invasive evaluation of vascular permeability	DCE-MRI = dynamic contrast-enhanced magnetic resonance image	199
Gd-CNDs@Fe_3O_4	Citric acid Ethanediamine $GdCl_3$	One-pot hydrothermal	Gd^{3+}	5.16	0.5	MRI/Fluorescence dual-mode imaging probe		132
N/Gd/Yb-CNDs	Citric acid Ethanediamine Gd^{3+} complex $YbCl_3$	One-pot microwave-assisted hydrothermal	Gd^{3+}/Yb^{3+}	5.02	7.0	MRI/CT/Fluorescence multi-mode imaging probe		137
Gd/Yb-CNDs	Na_2EDTA L-arginine $GdCl_3$ $YbCl_3$	One-pot hydrothermal	Gd^{3+}/Yb^{3+}	6.65	9.4	MRI/CT/Fluorescence multi-mode imaging probe		87
Gd-CNDs	Gd-DTPA Glycine	One-pot hydrothermal	Gd^{3+}	6.45	3.0	MRI/Radiotherapy		139
Gd-CNDs-Affibody	$Gd(NO_3)_3$ Gd-DTPA	Calcination	Gd^{3+}	2.55	3.0	MRI probe for tumour-targeting imaging		141
Ho-CNDs	Citric acid BPEI Ho-DTPA	Hydrothermal	Ho^{3+}	0.1128	1.5	MRI/Fluorescence dual-mode imaging probe		200
Ho-CNDs	Citric acid PEI $HoCl_3{\cdot}6H_2O$ DTPA	One-pot pyrolysis	Ho^{3+}	2.049	1.5	Molecular logic gate with pH responsivity to MR/Fluorescence signals		201